Computer Science Department of The University of Auckland
CITR at Tamaki Campus (http://www.tcs.auckland.ac.nz)

CITR-TR-20 May 1998

Shape from Shading and Photometric Stereo Methods

Reinhard Klette[1], Ryszard Kozera[2], and
Karsten Schlüns[3]

Abstract

This TR is a review of shading based shape recovery (shape from shading, photometric stereo methods). It reports about advances in appliedwork and about results in theoretical fundamentals.

[1] CITR, Tamaki Campus, University Of Auckland, Auckland, New Zealand
[2] Computer Science Department, University of Western Australia, Perth, Australia
[3] Pathology Institute, Charite, Humboldt University, Berlin, Germany

Shape from Shading and Photometric Stereo Methods

Reinhard Klette
The University of Auckland, Auckland, New Zealand
Ryszard Kozera
University of Western Australia, Perth, Australia
Karsten Schlüns
Humboldt University, Berlin, Germany

May 27, 1998

Abstract

This TR is a review of shading based shape recovery (shape from shading, photometric stereo methods). It reports about advances in applied work and about results in theoretical fundamentals.

1 Introduction

Reflectance based shape recovery of non-planar surfaces from one or several irradiance images is a classic task in computer vision [Horn 1986, Woodham 1978]. The goal is to reconstruct the three-dimensional shape of an object from its irradiances by using its reflection properties. The problem is called *Shape from Shading* (SFS) if just one irradiance image is used as input for the reconstruction process [Horn & Brooks 1989]. The term *photometric stereo method* (PSM) or just *photometric stereo* refers to the extension of Shape from Shading to a class of methods that use two (2S PSM) or more (3S PSM etc.) images for shading based 3D shape recovery.

A broad spectrum of techniques is available to approach reflectance based shape recovery in appropriate fields of application, see, e.g., [Klette et. al 1998]. For example, 3S PSM may be used for generating height maps of a human face, a human hand, etc., see Fig. 1. Using colored illumination [Drew 1994, Woodham 1994] this 3D reconstruction may be even achieved for dynamic scenes several times per second. The use of inexpensive equipment (three light sources and a video camera), not dangerous radiation (as in case of laser light) and a reasonable performance are three advantages of PSM. Furthermore, the image values of (one of) the acquired images may be used for texture mapping without any additional need to register height and texture data, because the generated height values are located at the same pixel position as the acquired image values.

Figure 1: Reconstructed face using photometric stereo.

This field of reflectance based shape recovery also contains serious mathematical problems (see e.g. proofs of existence or uniqueness of object surfaces [Kozera 1991], analysis of shadows or interrefections [Rumpel & Schlüns 1995, Schlüns 1997]). This TR reports about advances in applied and in theoretical work.

1.1 SFS and PSM

There are a number of factors that influence the measured irradiances of an image. Firstly, the image which is acquired by the sensor depends on the geometrical and spectral distribution of the light source which illuminates the observed scene. The individual objects of the scene are characterized by their geometry and by their reflection properties. The geometry and the reflection properties affect the light falling on the imaging sensor. The imaging system converts the light to measured image irradiances.

SFS methods try to infer the geometry of an object from a single image. For this inversion, the mentioned factors and their influences have to be considered for the conceptual design of a SFS method. The only a-prioi constraint is that only the geometry has to be extracted from the image. An additional goal could be to extract the reflection properties from the given image, as well, to obtain a more complete description of the visible surface.

It is impossible to infer unambiguous geometrical properties of objects from image irradiances without restricting the general problem. The design of SFS methods, that allow a mathematical proof of existence, uniqueness or conver-

gence of a solution, is a field of ongoing active research.

Common assumptions to ensure an unambiguous surface reconstruction from a single or several images are as follows:

(i) The *irradiance* E_0 and the *direction* $\mathbf{s}$ *of the illumination* are known. There are no intra-object or inter-object interreflections, i.e. scene objects do not act as secondary light sources. In general a light source is assumed which emits parallel light of a constant irradiance E_0 from a constant and known illumination direction $\mathbf{s} = (s_1, s_2, s_3)$. If the illumination direction $\mathbf{s}$ coincides with the viewer direction $\mathbf{v}$, i.e. $\mathbf{s} = (0, 0, -1)$, then SFS simplifies significantly. Some SFS methods exist that assume a close point light source, hence the light rays cannot be modeled as parallel. Approaches that assume diffuse illumination (e.g. sky illumination) form another special case. Furthermore, the effects of the inverse square law (see, e.g., [Klette et. al 1998]) are usually disregarded.

(ii) The *reflection properties of the object surfaces* are known. For additional simplification, linearly reflecting surfaces or Lambertian surfaces are often assumed where the *albedo* ρ is constant and known for the entire object.

(iii) The modeling by *reflectance maps* assumes that a unique scene radiance value is assigned to each *surface orientation* $\mathbf{n} = (n_1, n_2, n_3)$. Often the *reflectance map* is assumed to be known. For example it is assumed that the reflectance map can be approximated as being locally or globally linear.

(iv) For the *object surface geometry* it is assumed that faces can be approximated by continuous or continuously differentiable functions u in classes as C^1 or C^2. Some methods exist which are especially designed to reconstruct polyhedral objects. In general it has to be assumed that height values respectively orientations are known at a few (singular) points in advance. Of special interest are boundary points showing zero-irradiances (occluding boundaries) and points of maximal irradiance. Sometimes it is assumed that the surface can be locally approximated as a plane (facet model) or as a sphere.

(v) The *sensor* is linear.

(vi) Shading based shape recovery methods usually assume an orthographic *projection of scene objects* into the $xy-$image plane. This allows to consider surface functions $u(x, y)$ with first-order derivatives u_x, u_y, and normals $\mathbf{n} = (u_x, u_y, -1)$. There exist also methods that assume perspective projection.

These assumptions can be reduced by extracting some parameters from the scene which were expected to be known. For example, usually only the product of the irradiance E_0 of the light source and the albedo ρ has to be determined and not their individual values. Under the assumptions of parallel illumination, a Lambertian reflection, and an orientation $\mathbf{n}_0$ in the scene which coincides with

the illumination direction $\mathbf{s}$ it follows that the product $E_0\rho$ can be read from the maximal irradiance value. Also, in practice many of the constraints (except two of them) prove to be rather uncritical restrictions. The *critical assumptions* are that the albedo ρ is restricted to be constant over the whole object (or even over the whole image) which corresponds to a uniform coloring, and the limitation to Lambertian surfaces since beside the diffuse component many materials exhibit a considerable amount of specular reflection. A *genuine Lambertian surface* allows a representation by a graph of a function u.

Example 1 Assume parallel and constant illumination from lighting direction $\mathbf{s} = (s_1, s_2, s_3)$, a genuine Lambertian surface, constant albedo ρ, and a known product $E_0\rho$. According to *Lamberts cosine law* and the *image irradiance equation* it holds that

$$E = E_0\rho \cdot cos(\alpha) \tag{1}$$

with $\alpha = \angle(\mathbf{n}, \mathbf{s})$, for the measured irradiance E and a surface normal $\mathbf{n} = (u_x, u_y, -1)$. The term $cos(\alpha)$ and hence the angle α can be calculated from the known quantities. All vectors which subtend the angle α with the illumination direction are solutions to the above equation.

The *Gaussian sphere* is useful to represent these solutions. Without loss of generality we can restrict the surface orientations to *unit surface normals* $\mathbf{n}^\circ$. Then the solution vectors $\mathbf{n}^\circ$ form the lateral area of a right circular cone. The vertex of the cone lies at the center of the Gaussian sphere. The orientation of the cone (vector of the cone axis) is determined by the illumination direction $\mathbf{s}$. The boundary of the circular base of the cone is incident with the surface of the Gaussian sphere. All these points on the Gaussian sphere are surface orientations satisfying the equation for the image irradiance function E.

For *Lambertian surfaces* often we consider image irradiance equations

$$E_i(x,y) = \rho(x,y) \cdot \frac{u_x(x,y) \cdot p_i + u_y(x,y) \cdot q_i - r_i}{\sqrt{u_x(x,y)^2 + u_y(x,y)^2 + 1} \cdot \sqrt{p_i^2 + q_i^2 + r_i^2}} \tag{2}$$

defined over domains $\Omega_i = \{(x,y) \in \Re^2 : 0 \leq E_i(x,y) \leq 1\}$, for light sources $i = 1, 2, 3, ...$ with irradiances $E_{0,i} = 1$ and orientations (p_i, q_i, r_i), and image coordinates (x, y).

SFS methods are extended to PSM if several irradiances are known for every image point and the corresponding surface point. Because of the larger amount of data an improvement of the reconstruction results and furthermore a reduction of the necessary assumptions can be expected. Photometric stereo methods firstly recover surface orientations and can be combined with an integration method to calculate a *height* or *depth map*. Even without a subsequent integration step the surface orientations can be used, for example to determine curvature parameters of object surfaces or to recognize objects.

To acquire images for photometric stereo the object is consecutively illuminated by several light sources. Each image E_i is taken with only one light source

being switched on. A movement inside the system consisting of the object, the light sources, and the sensor is not allowed. Therefore, more than one irradiance value can be assigned to a projected surface point without encountering a correspondence problem. Each acquired image corresponds to one light source.

We distinguish between albedo dependent photometric stereo methods and albedo independent methods. The property of *albedo dependent methods* is that the albedo ρ of the surface material or the product $E_0\rho$ has to be known for every image point $(x, y.)$ This is especially true for all SFS methods. *Albedo independent methods* have the property that the albedo has theoretically no influence on the reconstruction of orientations or height values as long as $\rho > 0$.

1.2 Linear Sensor

Modern cameras suitable for image processing are usually based on semiconductor sensors the so-called CCD (*charge coupled device*) chips. Several properties of these cameras are of interest for the measuring process of irradiances, see, e.g., [Hashimoto et. al 1995].

A linear behavior of the imaging sensor is assumed in shading based techniques such as SFS, 2S PSM or 3S PSM. For these techniques it is assumed that the gray values (or the color values) in the image have a *direct linear relation* to the measured *image irradiances* (the radiation entering the camera lens). At first we briefly mention that signal attenuation caused by a pre-knee-circuit, clipping, and blooming already lead to a nonlinear camera response. Further reasons for nonlinear camera behavior are explained in the following and a sketch of a linearization technique is given.

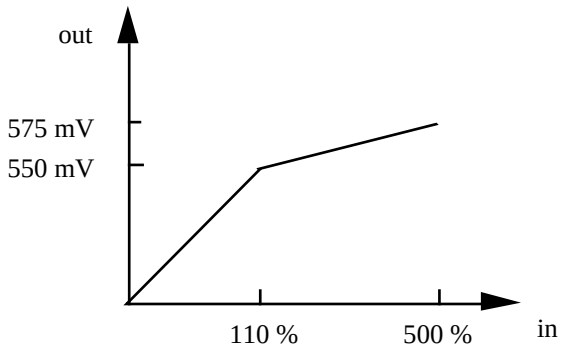

Figure 2: Example of pre-kneeing to preserve the dynamic range.

Attenuation of the signal occurs if more photons fall on the CCD chip than the image acquisition system is able to process. This can be caused by different factors when the image signal is processed in analog form (voltages) in the camera or when the signal is digitized in the frame grabber. One reason of attenuation is the limited *dynamic range* of the components in the imaging

system. The analog component of the camera system causes an attenuation if the electric signal is processed by a so-called *pre-knee-circuit*. Figure 2 shows the characteristics of the pre-knee-circuit of the Sony three chip camera DXC-930P. The voltage of the signal is linearly attenuated starting at a certain level of the input signal. As a result, the signal is not longer globally linear.

Furthermore, *clipping* of the input signal occurs whenever the analog signal exceeds the highest processable voltage, e.g. when the analog signal is converted to a digital signal (a gray value for each color channel) in the frame grabber. Usually, the clipping level (*white level*) of the analog/digital converter can be controlled by programming the frame grabber.

If the intensity of the incoming light at a CCD cell exceeds a certain level which is several times higher than the clipping level, it happens that the CCD cell is not able to accumulate more charge per time unit any longer. The additional charge is spread into the neighboring CCD cells. This effect is called *blooming* and appears as a white streak or blob around the affected pixels in the image. Blooming is particularly noticeable in scene analysis when specular highlights occur on the surface of the object that has to be reconstructed. For interline transfer sensors blooming starts at about 600 according to [Lenz 1989].

In principle CCD chips possess the property of having a high linearity because photons are transformed directly into charge in a CCD cell. But CCD cameras usually delinearize the signal for display requirements. It has to be guaranteed that the light received by the camera is transformed into a proportional amount of light emitted by a monitor screen. The input voltage U of a cathode ray tube in a monitor and the emitted radiant intensity I are in exponential relationship $I \approx U^{\gamma}$ where γ is the *gamma value*. Therefore, a circuit is integrated in the camera for the *gamma correction*. The circuit adjusts the *linear* CCD camera signal U_{in} to the *nonlinear* monitor characteristic

$$U_{out} = U_{max}^{(1-1/\gamma)} \cdot U_{in}^{1/\gamma} \tag{3}$$

where U_{max} is the maximum voltage. The gamma value γ depends on the monitor and the video standard of the television system.

Therefore, the gamma correction has to be inverted to linearize the camera characteristic. This gamma re-correction can be done through substituting γ by $1/\gamma$ if the gamma value of the camera is known. This leads to the equation

$$E_{out} = G_{max}^{(1-\gamma)} \cdot E_{in}^{\gamma} \tag{4}$$

which transforms the measured image irradiance values (gray values) from E_{in} to E_{out}. For many CCD cameras it is possible to switch the gamma value through the camera control unit to 1. This avoids a gamma re-correction procedure.

If neither the gamma value is known nor the gamma correction can be switched off then the gamma value has to be calculated by using a calibration image. A calibration image for this purpose usually contains a number of gray and/or matte color patches of known reflection properties, see

[McCamy et. al 1976, Meyer 1988] for one example of a calibration chart. The spectral reflectance factors of gray patches of such a calibration chart are constant over the visible wavelength interval of the light. The constant reflectance factors (*albedos*) can be represented as percentages which describe how much light the gray patches reflect. The percentages are properties of the patches and are independent from the illumination and the camera. The relationship between these percentages and the measured image irradiances describes directly the camera behavior with respect to linearity. Since a model of the nonlinear characteristic of the camera is known (see formula above) the gamma value can be estimated.

Besides the gamma correction which causes a nonlinear camera behavior the *black level* has to be considered. A CCD cell generates electrons even if no light (photons) are falling on the light sensitive area which arise from thermal energy within the CCD chip. The current generated by these electrons is called *dark current*. The analog/digital converter transforms the associated voltage into an image gray value (measured image irradiance). The gray value which is a result of the dark current is called *black level*. It can be modeled as being an additive offset to the camera signal and must be subtracted from the gray values. Actually the black level does not lead to a nonlinear characteristic but the goal is to produce a camera curve that is directly linear that means a totally black gray patch having 0% reflection should generate the gray value 0. Often the black level can be adjusted by a knob at the camera control unit called master black control.

A further factor playing an important role with respect to color reproduction is the overall scaling of the three color channels. A gray object taken under white illumination produces a gray image, hence the color channels have identical gray values v. Therefore, the gray value triple $\mathbf{C} = (v, v, v)$ is assigned to each pixel when we assume idealized image acquisition. Although called "white", the color of white light sources, such as daylight, fluorescent lamps, and usual light bulbs produce different white tones, expressed in color temperature values. To get "white" for these different light sources a so-called *white balance* has to be performed. A manual white balance is done by exposing a white object to the color camera and pushing the white balance button at the camera control unit.

1.3 Illumination Parameters

The 3S PSM approach (as discussed later on) can also be employed for the calculation of an *illumination direction*, see [Horn 1986]. Assume that we have acquired the irradiance images of a curved calibration object having a Lambertian surface of known geometry (e.g. a sphere) and having uniform albedo ρ.

The 3S PSM assumes that three positive irradiance values $\mathbf{E} = (E_1, E_2, E_3)$ can be measured for every image point (x, y) with respect to three illumination directions $\mathbf{p}$, $\mathbf{q}$, and $\mathbf{r}$. 3S PSM is then directed on calculating a (unit) surface normal $\mathbf{n}^\circ$ from such an irradiance triplet by using the known illumination parameters.

Now we consider one point light source. For the calculation of one illumination direction $\mathbf{s}$ the calibration object has to ensure (at least) three depicted and illuminated surface points with known and non-coplanar surface (unit) normals $\mathbf{n_1}^\circ$, $\mathbf{n_2}^\circ$, and $\mathbf{n_3}^\circ$. These three known surface normals are combined into a matrix

$$\mathbf{N} = \begin{pmatrix} \mathbf{n}^\circ_{1x} & \mathbf{n}^\circ_{1y} & \mathbf{n}^\circ_{1z} \\ \mathbf{n}^\circ_{2x} & \mathbf{n}^\circ_{2y} & \mathbf{n}^\circ_{2z} \\ \mathbf{n}^\circ_{3x} & \mathbf{n}^\circ_{3y} & \mathbf{n}^\circ_{3z} \end{pmatrix}.$$

Assume furthermore a diagonal matrix $\mathbf{D}$ which contains in its diagonal positions the irradiance values of the light source at the considered image points. In practice we can assume that these light source irradiances are constant over the object, i.e. $\mathbf{D}$ contains the same positive value in all three diagonal positions. This leads to the following system of *image irradiance equations*

$$\mathbf{E}^T = \rho \cdot \mathbf{D} \cdot \mathbf{N} \cdot \mathbf{s}^\circ. \tag{5}$$

The unit vector of the illumination direction which is scaled by the albedo ρ can be determined with

$$\mathbf{s}^\circ = \mathbf{N}^{-1} \cdot \frac{1}{\rho}\mathbf{D}^{-1} \cdot \mathbf{E}^T. \tag{6}$$

This shows that in practice the matrix $\mathbf{D}$ can simply be the identity matrix. Because the meaning of being given or unknown data is exchanged for the surface normals and the illumination directions in comparison to 3S PSM this method is also referred to as *inverse 3S PSM*. The robustness can be improved by including more than three surface normals.

1.4 Theoretical Fundamentals

Approaches in shading based shape recovery transform measured irradiance values into data about surface functions u. These transformations are based on models about light sources, sensors, surface geometry or surface reflectance. Within a given context the theoretical fundamentals are specified by problems as

(i) existence of solutions u within a class of surface functions (as C^1 or C^2, or convex surfaces) and with respect to used models,

(ii) uniqueness of solutions u,

(iii) analytic or geometric relationships between several solutions (as possible decompositions into "similar" components),

(iv) methods for calculating such solutions u,

(v) algorithms for implementing such methods, and

(vi) features of these algorithms as stability, domain of influence, or convergence of iterative solutions towards the proper solution u.

The following sections of this TR contain results related to topics (i) ... (v). As an illustration to results to topic (vi) we discuss briefly the convergence of algorithms for *linear SFS*, see [Kozera & Klette 1997].

We assume discrete irradiance values $E(x, y)$ at exactly all grid point positions within a rectangular domain Ω. The grid resolution is specified by a grid constant 2^{-r}, for $r = 0, 1, 2, ...$ and the resulting grid points are called *r-grid points*. We assume $N_r \times N_r$ r-grid points in Ω, say with $N_r = 2^r \cdot (N_0 + 1) - 1$. These measured image irradiances are assumed to correspond to reflectance properties of a projected object surface satisfying a *linear image irradiance equation*

$$a \frac{\partial u}{\partial x}(x, y) + b \frac{\partial u}{\partial y}(x, y) = E(x, y) . \tag{7}$$

We assume an integrable function u on Ω and $(a, b) \neq (0, 0)$. The task is to calculate a function u over Ω based on the available input set of discrete irradiance values $E(x, y)$ at r-grid points, and based on a specified boundary condition, where u satisfies equation(7).

More precisely, we are interested in a numerical solution of the following *Cauchy problem*: If $sgn(ab) \geq 0$ then

$$u(x, 0) = f(x), \quad \text{for} \quad 0 \leq x \leq N_0 + 1$$

is given as boundary condition, and if $sgn(ab) < 0$ then

$$u(x, N_0 + 1) = f(x), \quad \text{for} \quad 0 \leq x \leq N_0 + 1$$

is given. Furthermore also

$$\chi(0, y) = g(y) , \quad \text{for} \quad 0 \leq y \leq N_0 + 1$$

is assumed to be known. The functions f, g are integrable on $[0, N_0 + 1]$ and satisfy $f(0) = g(0)$ if $sgn(ab) \geq 0$, or $f(0) = g(N_0 + 1)$ if $sgn(ab) < 0$.

This Cauchy problem is given in "digital form", i.e. only values at r-grid point positions are given for functions $p = u_x$, $q = u_y$, E, f, and g.

A linear partial differential equations may be solved with the aid of the finite difference method. Assuming normed function spaces on Ω the sequence of r-grids allows us to define corresponding normed r-grid spaces, for details see [Kozera & Klette 1997]. A *finite difference scheme* (FDS) is defined for all r-grids, for $r = 0, 1, 2, ...$, and basically it characterizes an operator R_r mapping an unknown function defined on Ω, as u in our case, into a function u_r,

$$R_r(u) = u_r, \quad \text{with} \quad u_r(i, j) \approx u(i \cdot 2^{-r}, j \cdot 2^{-r})$$

defined on r-grid points which is considered to be an approximation of the unknown function.

For example, applying a (simple) *forward difference approach* together with Taylor's expansion yields

$$\left.\frac{\partial u}{\partial x}\right|_r^{(i,j)} = \frac{u_r(i+1,j) - u(i,j)}{2^{-r}} + O\left(2^{-r}\right)$$

in the x-direction, and

$$\left.\frac{\partial u}{\partial y}\right|_r^{(i,j)} = \frac{u_r(i,j+1) - u(i,j)}{2^{-r}} + O\left(2^{-r}\right)$$

in the y-direction. A (simple) *backward difference approach* in x-direction is given by

$$\left.\frac{\partial u}{\partial x}\right|_r^{(i,j)} = \frac{u(i,j) - u(i-1,j)}{2^{-r}} + O\left(2^{-r}\right),$$

just to mention a further example. The differences are normalized by the distance 2^{-r} between neighboring r-grid points, in x- or in y-direction. Larger neighborhoods could be used for defining more complex forward or backward approaches, and further approaches may also be based on symmetric, or unbalanced neighborhoods of r-grid points. Finally, a finite difference scheme is characterized by selecting one approach for the $x-$, and an other one for the y-direction.

The *forward-forward FDS* transforms the given differential equation into

$$a \cdot \frac{u_r(i+1,j) - u_r(i,j)}{2^{-r}} + b \cdot \frac{u_r(i,j+1) - u_r(i,j)}{2^{-r}} + O\left(2^{-r}\right) = E\left(i2^{-r}, j2^{-r}\right),$$

and this equation may be simplified as

$$\tilde{u}_r(i,j+1) = \left(1 + \tfrac{a}{b}\right) \cdot \tilde{u}_r(i,j) - \tfrac{a}{b} \cdot \tilde{u}_r(i+1,j) + \tfrac{2^{-r}}{b} \cdot E\left(i2^{-r}, j2^{-r}\right),$$

where $\tilde{u}_r(i,j)$ is used as an approximation for function $u_r(i,j)$. The *backward-forward FDS* leads to

$$\tilde{u}_r(i,j+1) = \left(1 - \tfrac{a}{b}\right) \cdot \tilde{u}_r(i,j) + \tfrac{a}{b} \cdot \tilde{u}_r(i-1,j) + \tfrac{2^{-r}}{b} \cdot E\left(i2^{-r}, j2^{-r}\right),$$

the *forward-backward FDS* leads to

$$\tilde{u}_r(i+1,j) = \left(1 - \tfrac{b}{a}\right) \cdot \tilde{u}_r(i,j) + \tfrac{b}{a} \cdot \tilde{u}_r(i,j-1) + \tfrac{2^{-r}}{a} \cdot E\left(i2^{-r}, j2^{-r}\right),$$

and the *backward-backward FDS* leads to

$$\tilde{u}_r(i,j) = \tfrac{1}{1+c} \cdot \tilde{u}_r(i,j-1) + \tfrac{c}{1+c} \cdot \tilde{u}_r(i-1,j) + \tfrac{2^{-r}}{b(1+c)} \cdot E\left(i2^{-r}, j2^{-r}\right),$$

where $c = \frac{a}{b} \neq -1$, and to

$$\tilde{u}_r(i-1,j) = \tilde{u}_r(i,j-1) + \tfrac{2^{-r}}{b} \cdot E\left(i2^{-r}, j2^{-r}\right)$$

otherwise for $c = -1$. These schemes were studied in [Kozera & Klette 1997].

A finite difference scheme is *consistent* with an initial boundary value problem if the error of approximation in representing the original problem converges to zero as $2^{-r} \to 0$. The listed four schemes are consistent.

A finite difference scheme is *convergent* to the solution u_r (if it exists) if the digitization error converges to zero as $2^{-r} \to 0$. A further notion of stability for linear difference schemes was defined by *Rjabenki* and *Filippov*. A linear difference scheme is *RF stable* if the operators

$$\left\{R_r^{-1}\right\}_{r=0,1,2,\ldots}$$

are *uniformly bounded* as $2^{-r} \to 0$. A consistent and RF stable finite difference scheme is convergent to the solution of the given Cauchy problem if such a solution exists.

For the convergence analysis of the given schemes let $c = \frac{a}{b}$ assuming that $b \neq 0$, and $d = \frac{b}{a}$ assuming that $a \neq 0$.

Theorem 1 [Kozera & Klette 1997] *The forward-forward FDS is RF stable iff* $-1 \leq c \leq 0$. *The backward-forward FDS is RF stable iff* $0 \leq c \leq 1$. *The forward-backward FDS is RF stable iff* $0 \leq d \leq 1$. *The backward-backward FDS is RF stable iff* $c \geq 0$ *or* $c = -1$.

Consequently, in these positive cases the sequences of functions

$$\{\tilde{u}_r\}_{r=0,1,2,\ldots}$$

are convergent to the solution of the specified Cauchy problem.

2 Reflection and Gradients

The amount of light encoded into the gray value of a particular pixel of a digital image can be seen as the result of interactions between surface materials and light sources. Vision based shape recovery methods are influenced by the lighting and by the reflection characteristics of the observed objects. Therefore it is necessary to model the properties of both the illumination and the object materials. A discussion of radiometric and photometric quantities which are relevant to computer vision is offered by [Haralick & Shapiro 1993, Klette et. al 1998]. Vision based shape recovery normally leads to reconstructions of gradient maps. These gradient maps have to be integrated for generating depth or height maps. This section deals with reflection models [Schlick 1994] and gradient integration. Both topics are interesting subproblems in shading based shape recovery.

2.1 Reflectance-Distribution Functions and Reflectance Maps

The *bidirectional reflectance-distribution function* (BRDF) describes reflection characteristics. The BRDF was defined in 1977 [Nicodemus et. al 1977] by the

National Bureau of Standards, USA, for the standardization of reflection representations. The BRDF describes how "bright" a differential surface dA of a material appears when it is observed from a general direction and illuminated from a particular direction, see Fig. 3. The BRDF

$$f_r\left(\theta_2, \phi_2; \theta_1, \phi_1\right) = \frac{dL_1\left(\theta_2, \phi_2; \theta_1, \phi_1; E_2\right)}{dE_2\left(\theta_2, \phi_2\right)} \tag{8}$$

is defined as the ratio between the reflected differential radiance dL_1 in viewer direction and the differential irradiance dE_2 coming from an illumination direction. The BRDF is expressed in sr^{-1} (1/steradian). The term "direction" in this definition should be interpreted as a differential solid angle in a direction given by spherical coordinates. The letter θ denotes the slant angle and the letter ϕ stands for the tilt angle. The spherical coordinates of the BRDF refer to a right-handed coordinate system where the origin coincides with the surface point and whose z-axis coincides with the surface orientation. The tilt angle is taken counterclockwise by looking onto the surface patch.

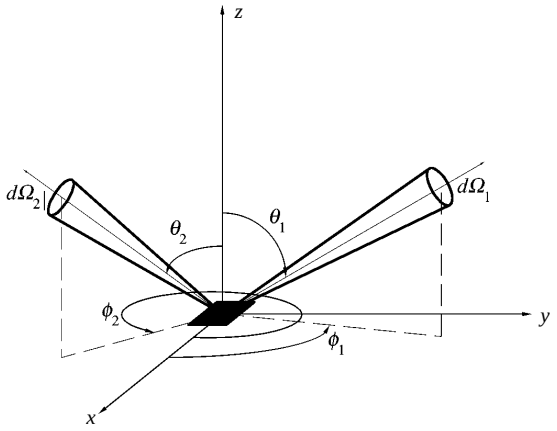

Figure 3: Geometry of the bidirectional reflectance-distribution function (BRDF).

If the differential irradiance dE_2 is described in the foreshortened portion of the illumination over the differential solid angle $d\Omega_2$ by using the radiance which is received by the surface the BRDF can be formulated as

$$f_r\left(\theta_2, \phi_2; \theta_1, \phi_1\right) = \frac{dL_1\left(\theta_2, \phi_2; \theta_1, \phi_1; E_2\right)}{L_2\left(\theta_2, \phi_2\right) \cdot \cos(\theta_2)\, d\Omega_2}. \tag{9}$$

If we integrate over the entire observed solid angle Ω_2 of the incoming radiation the reflected radiance L_1

$$L_1 = \int_{\Omega_2} f_r\left(\theta_2, \phi_2; \theta_1, \phi_1\right) \cdot L_2\left(\theta_2, \phi_2\right) \cdot \cos(\theta_2)\, d\Omega_2 . \tag{10}$$

The irradiance dE_2 depends on a direction since it holds

$$dE_2\left(\theta_2, \phi_2\right) = L_2\left(\theta_2, \phi_2\right) \cdot \cos(\theta_2)\, d\Omega_2 . \tag{11}$$

A *perfectly diffuse* reflecting surface appears equally bright when observed from any arbitrary direction. Furthermore, this feature is also independent from the type of illumination. If a surface emits the entire incoming energy through reflection then it is called a *Lambertian reflector* and neither absorption nor transmission of radiation takes place. It follows that the entire radiance L_1 which is reflected over the visible hemisphere is equal to the incoming irradiance E_2. A Lambertian reflector has three important properties:

(i) The reflected radiance L_1 does not depend on the direction (isotropic) and is constant, i.e. $L_1\left(\theta_1, \phi_1\right) = L_1 = const.$

(ii) The BRDF is constant, i.e. $f_r\left(\theta_2, \phi_2, \theta_1, \phi_1\right) = f_r = const.$

(iii) The radiant emittance M is equal to the irradiance E_2.

The radiant emittance M can now be expressed as the integral of the reflected radiance L_1 over the visible hemisphere:

$$M = \int_{\Omega_1} L_1\, d\Omega_1 = L_1\, \pi = E_2. \tag{12}$$

From this it follows that

$$f_r = \frac{L_1}{E_2} = \frac{1}{\pi} \tag{13}$$

holds for the Lambertian reflector. If the Lambertian reflector is illuminated by a light source which has the radiance $L_2(\theta_2, \phi_2)$ we get

$$L_1 = \frac{1}{\pi} \int_{\Omega_2} L_2(\theta_2, \phi_2) \cdot \cos(\theta_2)\, d\Omega_2 \tag{14}$$

as reflected radiance. This equation contains *Lamberts cosine law*

$$L_1 = \frac{E_0}{\pi} \cdot \cos(\theta_2) \tag{15}$$

for the reflected radiance L_1 of a Lambertian reflector illuminated by a parallel radiating light source of irradiance E_0. The index 0 usually denotes a quantity related to the light source. It is assumed that illumination directions outside of the interval

$$0 \leq \theta_2 < \frac{\pi}{2} \tag{16}$$

do not cause reflections.

According to its definition the Lambertian reflector does not absorb any radiation for any wavelength. The *albedo* ρ is used to describe surfaces which possess all properties of a Lambertian reflector apart from a partial absorption of the incoming radiation (*Lambertian surfaces*). It describes the relative portion of the radiation which is reflected by the surface. The albedo can be seen as a scaling factor which lies usually in the interval $[0, 1]$. The definition of the albedo can be extended to non-Lambertian surfaces.

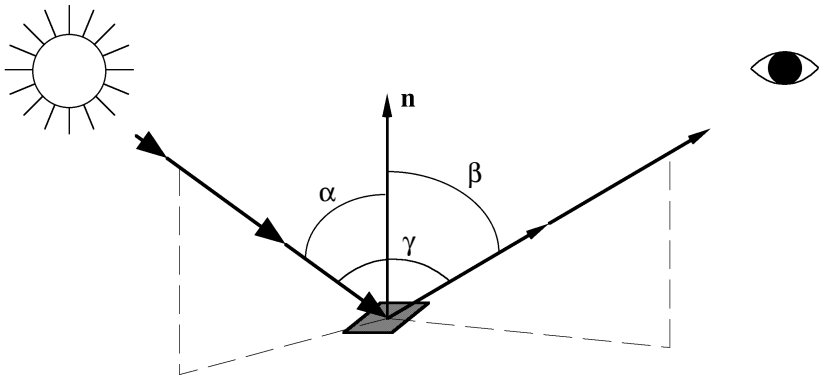

Figure 4: Definition of three photometric angles α, β, and γ. Each arrow marks the direction of one light ray.

The three *photometric angles* α, β, and γ are defined with respect to the surface normal $\mathbf{n}$ (see Fig. 4) where α is the angle between the surface normal and the illumination direction (*incident angle*), β is the angle between the surface normal and the reflection direction (*emittance angle*), and γ is the angle between the illumination direction and the reflection direction (*phase angle*). Without loss of generality the reflection direction can be aligned to the viewer direction (optical axis of sensor).

The viewer direction is described by a vector $\mathbf{v}$ which points to the viewer (camera). Generally, an orthographic projection is assumed so that the viewer direction reduces to $\mathbf{v} = (0, 0, -1)$. This is the standard viewer direction. The illumination direction is also simply described by a vector $\mathbf{s}$ which points to the light source.

The radiance equation for a Lambertian reflector can be extended for a *general Lambertian surface* not being necessarily a Lambertian reflector. Let us assume that the surface has albedo ρ and is illuminated by a parallel radiating light source with irradiance E_0 under the incident angle α. Then the corresponding radiance equation is

$$L_1 = \frac{E_0}{\pi} \cdot \rho \cdot \cos(\alpha) = \frac{E_0}{\pi} \cdot \rho \cdot \cos \angle (\mathbf{n}, \mathbf{s}) . \tag{17}$$

Considering surface reflection properties and assuming non-varying illumination directions $\mathbf{s}$ and viewer directions $\mathbf{v}$ variations in the reflected radiation are solely caused by changes of the surface orientation. [Horn 1977] introduced the *reflectance map* to model this relationship. Reflectance maps can be defined as continuous or discrete functions. Usually the *gradient space* representing the surface gradients $(p, q) = (u_x, u_y)$ is chosen for reflectance maps because of its simplicity. In this case the reflectance map function is $R(p, q)$. Another useful representation are stereographic coordinates (f, g) and reflectance maps $R_s(f, g)$. Furthermore, a general reflectance map $R_n(\mathbf{n}^\circ)$ can be defined by using the unit surface normal $\mathbf{n}^\circ$. As an example,

$$R(p, q) = E_0 \cdot \rho \cdot \frac{s_1 \cdot p + s_2 \cdot q - s_3}{\|(s_1, s_2, s_3)\|} \tag{18}$$

is a *linear reflectance map*, for illumination direction $\mathbf{s} = (s_1, s_2, s_3)$ and using gradient space representation. The shading of a sphere that has linear reflectance is shown in Fig. 5.

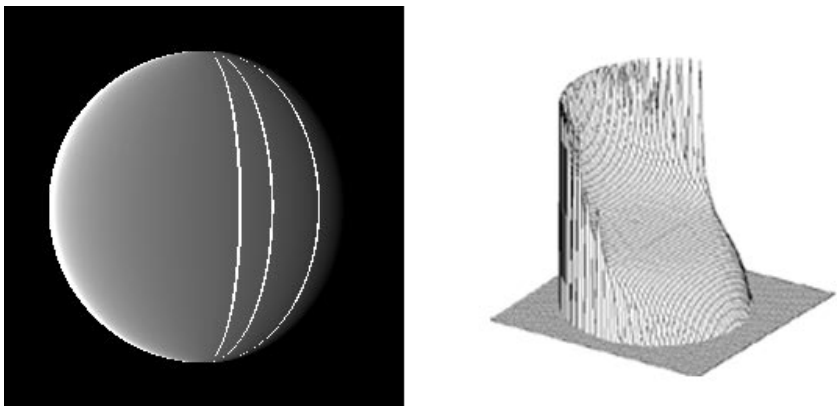

Figure 5: Irradiance image of a linearly shaded sphere using the illumination orientation $\mathbf{s} = (-0.5, 0, -1)$, and three overlaid isoirradiance curves (left) and a grid representation of the irradiances (right).

Constant scaling factors are usually eliminated from the representation of reflectance maps, as the factor $1/\pi$ for the Lambertian reflectance maps. Consequently, the reflectance map

$$R\left(p,q\right) = E_0 \cdot \rho \cdot \cos \angle \left(\left(p,\ q,\ -1\right),\ \mathbf{s}\right) \tag{19}$$

$$R_s(f,g) = E_0 \cdot \rho \cdot \frac{\left(4f,\ 4g,\ f^2+g^2-4\right) \cdot \mathbf{s}^\circ}{4+f^2+g^2}, \tag{20}$$

or

$$R_n\left(\mathbf{n}^\circ\right) = E_0 \cdot \rho \cdot {\mathbf{n}^\circ}^T \cdot \mathbf{s}^\circ \tag{21}$$

corresponds to a Lambertian surface (see Fig. 6). A *rotationally symmetric Lambertian reflectance map* is given by

$$R\left(p,q\right) = E_0 \cdot \rho \cdot \frac{1}{\|(p,\ q,\ -1)\|}, \text{ where } \mathbf{s} = \mathbf{s}^\circ = \mathbf{v} = \mathbf{v}^\circ = (0,\ 0,\ -1)^T\ . \tag{22}$$

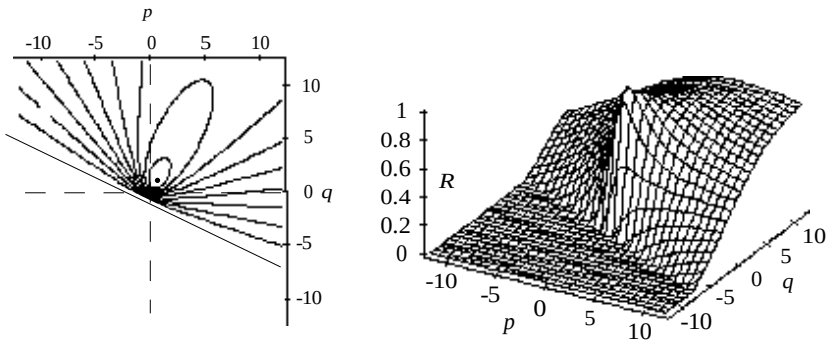

Figure 6: Reflectance map of a Lambertian surface in gradient space with illumination direction $\mathbf{s} = (0.5, 1, -1)$. Left: isoradiance contour plot. Right: three-dimensional plot.

Lambertian reflectance maps with $\mathbf{s} \neq \mathbf{v}$ are not rotationally symmetric. The left hand side of Fig. 6 shows the reflectance map as isoradiance plot thus every curve shows orientations of equal scene radiance values (*isoradiance curves*). The second order isoradiance curves in these maps describe a point, a circle, an ellipse, a parabola, a hyperbola, or a straight line. Every isoradiance curve

defines the location of equal irradiances in a captured image. Consequently, these curves are also called *isoirradiance curves*.

The point in the isoradiance plot represents that gradient which is identical to the gradient (p_s, q_s) of the illumination direction and hence takes the maximal radiance value. The gradients lying on the straight line represent those surface normals which are orthogonal to the illumination direction. The function value zero is assigned to them since surface patches oriented in this way cannot receive light from the light source. This straight line is called *self-shadow line*.

It holds an algebraic duality that the distance between the illumination gradient (p_s, q_s) and the origin is reciprocal to the distance between the self-shadow line and the origin. The illumination gradient and the self-shadow line are located on different sides of the origin. It follows that the self-shadow line is uniquely defined by the illumination gradient. The self-shadow line is called the *dual line* to this gradient.

For isotropically reflecting surface materials with unknown reflection characteristics the mapping of an orientation to a radiance value can be determined using a calibration object, see [Klette et. al 1998]. The following assumptions are made: the calibration object has the same surface material as the surface which has to be reconstructed later on by using SFS or PSM. Note that only one surface material can be characterized by a single reflectance map.

2.2 Reflection and Image Irradiance Equation

The simple reflection representation in the form of reflectance maps allows the description of the large class of isotropic reflecting materials.
However for more general cases it is of benefit to use analytical reflection models in a more general way than already done for the Lambertian reflection [Nayar & Oren 1995]. An analytical reflection model should satisfy the requirements of simplicity and should be physically plausible as much as possible. In general, *hybridly reflecting surfaces* have to be considered where reflection is an additive composition of *diffuse* or *body reflection* L_b and of *specular* or *interface reflection* L_s.

The diffuse reflection component is usually modeled by Lamberts cosine law though there exists no complete physical explanation of Lamberts cosine law. In contrast many models exist for the description of the specular reflection component. In principle there are two different ways to describe specular reflection, approaches that use physical optics (wave optics) and approaches which apply models from geometrical optics [Hecht 1997]. Approaches of physical optics use the electromagnetic theory for the analysis of the reflection where the Maxwell equations constitute the mathematical basis. The application of geometrical optics is a lot simpler, but it can be used only if the wavelength of the incoming light is small compared to the roughness of the material. Consequently, reflection models which are derived from geometrical optics can always be approximations of the wave-optical reflection models. Two general representatives of these approaches are the Beckmann-Spizzichino model (physical optics) and the Torrance-Sparrow model (geometrical optics), see [Nayar et. al 1991]. Sim-

plifications of both reflection models are used in computer vision and computer graphics to describe the specular component.

The *Beckmann-Spizzichino model* describes the specular reflection by two additively overlapping components usually called specular spike and specular lobe. The specular spike-component models a portion of the reflection which only occurs in a very narrow range of angles around the direction of perfect specular (mirror-like) reflection. The diffuse portion of the specular reflection is modeled by the lobe component. It describes the scattering reflection caused by the surface roughness.

The *Torrance-Sparrow model* describes the specular reflection for surfaces whose roughness is large compared to the wavelength of the light. It models the surface by planar, perfectly specular reflecting microfacets whose orientations are normally distributed around the macroscopic surface orientation which is visually inferable. The mathematical formula mainly comprises a Fresnel term, the geometrical attenuation factor, and a Gaussian normal distribution. The Fresnel term describes the reflection behavior depending on the illumination direction $\mathbf{s}$, on the viewer direction $\mathbf{v}$, and on the refraction index of the surface material. Note that the refraction index depends on the wavelength. Besides a simplified Torrance-Sparrow model the *Phong model* is used in computer vision and in computer graphics [Foley et. al 1990].

A model that describes hybrid reflection properties without specifying the diffuse and the specular reflection component explicitly is the *Dichromatic Reflection Model* (DRM). This model, see [Klinker et. al 1990], can be used for inhomogeneous dielectric materials whose surface structure can be modeled as being composed of an interface and an optically neutral medium containing color pigments. Figure 7 illustrates the principal structure of such an inhomogeneous dielectric.

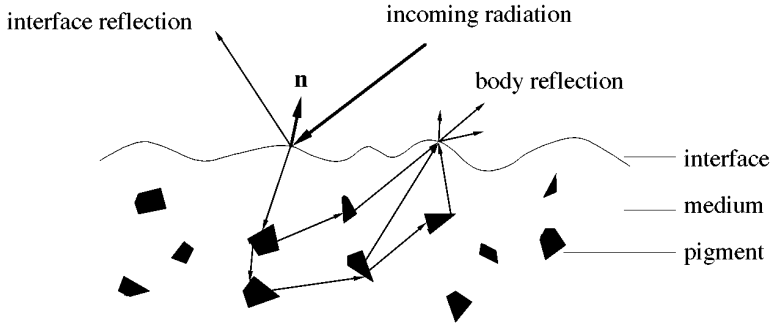

Figure 7: Simple model of an inhomogeneous dielectric material.

The interface separates the surface from the environment which is usually air. If the distribution of the color pigments is uniform and the pigments display the same optical behavior then it can assumed that the penetrating light does not

have a specific direction when it leaves the surface (body or diffuse reflection). Part of the radiation falling on the object surface does not penetrate the medium and is reflected by the interface (interface or specular reflection). The DRM models the specular reflection component with microfacets. Mathematically, the DRM can be formulated in the following way:

$$\begin{aligned} L(\lambda, \mathbf{n}, \mathbf{s}, \mathbf{v}) &= L_s(\lambda, \mathbf{n}, \mathbf{s}, \mathbf{v}) + L_b(\lambda, \mathbf{n}, \mathbf{s}, \mathbf{v}) \\ &= m_s(\mathbf{n}, \mathbf{s}, \mathbf{v}) \cdot c_s(\lambda) + m_b(\mathbf{n}, \mathbf{s}, \mathbf{v}) \cdot c_b(\lambda) \end{aligned} \tag{23}$$

where the modeled scene radiance L is a quantity that depends on the wavelength λ.

The essential assumption of the DRM is that both reflection components can be factorized into a geometrical component and a spectral component as given in the above formula. The geometrical components are m_s and m_b. The spectral components are c_s and c_b. The factor c_s is called *interface reflection color* and c_b is the *body reflection color*. The factorization of the interface reflection only holds under specific assumptions [Klette et. al 1998]. The factorization of the body reflection is feasible without any further significant restrictions.

With the additional assumption of a neutral reflecting interface, c_s describes the spectral distribution (color) of the light source. This special case of the DRM is called *Neutral Interface Reflection Model* (NIRM). The geometrical component m_s can be made explicit by the formulas of a simplified Torrance-Sparrow model, the Phong model or other models. But the particular advantage of the DRM is that the geometric component of the specular reflection does not have to be modeled explicitly to apply the DRM for various tasks. The scaling factor m_b can be usually modeled by Lamberts cosine law.

If the description of the scene radiance L is restricted to three narrow wavelength bands in the red, green, and blue spectral range of the visible light then the scene radiance can be represented as a three-dimensional color vector

$$\mathbf{L} = m_s(\mathbf{n}, \mathbf{s}, \mathbf{v}) \cdot \mathbf{c}_s + m_b(\mathbf{n}, \mathbf{s}, \mathbf{v}) \cdot \mathbf{c}_b. \tag{24}$$

Since, from the mathematical point of view, m_s and m_b represent arbitrary scaling factors the vectors $\mathbf{c}_s$ and $\mathbf{c}_b$ form a two-dimensional sub-space (a plane) in the RGB color space (*dichromatic plane, color-signal plane*).

It can be observed that the colors in the dichromatic plane form T- and L-shaped clusters if the object has sufficiently many and different surface orientations. Figure 8 shows on the left the outline of a typical L-shaped cluster and on the right the cluster for the real orange watering can (see Fig. 9, left). If the object shows several hybridly reflecting materials one cluster arises for every material. The representations shown in Fig. 8 are called *color histograms*. Contrary to gray value histograms color histograms only have binary values. Color histograms only code whether a certain color exists in the image or not. Both the DRM and the NIRM are of great importance in physics-based computer vision.

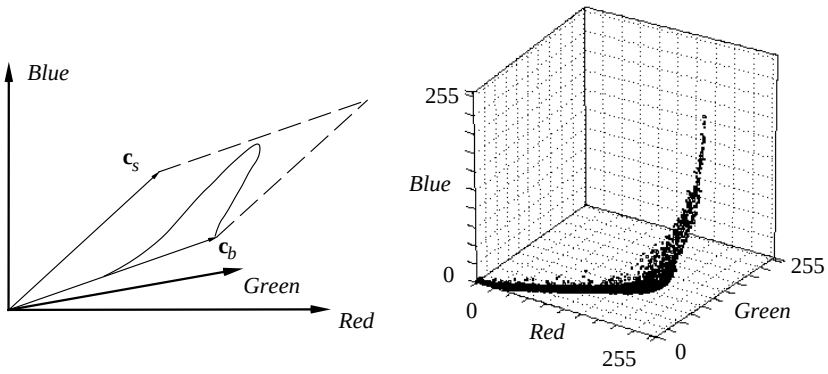

Figure 8: Left: Dichromatic plane of a curved, hybridly reflecting object showing one color. Right: An L-shaped color cluster of a real watering can (see Fig. 9, left).

For example, it is possible to separate the reflection components and hence to remove the specular reflection component (highlights) from images by analyzing color histograms [Klinker et. al 1988, Klinker et. al 1990, Schlüns 1997].

Figure 9 displays an example of such a highlight removal. The left picture shows the original image of a watering can. The right picture shows the watering can after the elimination of the specular reflection component using the DRM. These reflection models can also be used to remove interreflections [Rumpel & Schlüns 1995], for color image segmentation, color classification, and color object recognition.

Now we discuss the relation between the radiance reflected from the object surfaces (scene radiance) to its counterpart, the measured image irradiance of the imaging sensor. It can be shown [Horn & Sjoberg 1979] that (under a few assumptions, see also [Klette et. al 1998]) the relation between the reflected radiance L and the image irradiance E can be approximated by

$$E = L \cdot \frac{\pi}{4} \cdot \frac{d^2}{f^2} \cdot \cos^4(\psi) \tag{25}$$

where d is the diameter of the lens, f is its focal length and ψ is the angle between the optical axis and the light ray going through the center of the observed small solid angle.

This relationship in conjunction with a reflectance map R leads to the *image irradiance equation*

$$E\,(x,\,y) = c \cdot R\,(p,\,q)\;, \tag{26}$$

Figure 9: Left: image of a real watering can showing a large highlight. Right: picture of the watering can after removal of the specular reflection. The six gray patches in the bottom line were used to linearize the camera (compare Section 1.2).

where c is a scaling factor. Since the surface gradient (p, q) depends on world coordinates but the image irradiance E is given in terms of image coordinates, this equation implicitly contains the assumption of an orthographic projection as it was already assumed for defining the reflectance map.
If, additionally, the image irradiance is proportional to the values measured by the imaging sensor and the digitization system then the relationship between the scene radiance and the measured image irradiance (gray value) of the image is linear, too. Normal video cameras have a built-in gamma recorrection (compare Section 1.2) which is a non-linear mapping between the image irradiances and the gray values. Therefore a photometric calibration must be carried out to linearize the camera before the image irradiance equation can be applied. For simplification purposes the image irradiance equation is often represented in the literature by

$$E\,(x,\,y) = R\,(p,\,q)\,. \tag{27}$$

Therefore the function $E(x, y)$ in this equation can be regarded as image irradiance function and as measured image irradiance function. The image irradiance equation is the most important tool to describe the relationship between irradiances, scene radiances, and surface gradients.

2.3 Depth Maps from Gradient Maps

Besides the models of surface reflection models of surface geometry are also used in shading base shape recovery. Classes of C^n *functions* are suitable to describe

curved surfaces. These classes model continuity respectively differentiability assumptions. Generally $C^n(\Omega)$ denotes the class of all functions that are defined on a domain Ω, for $n \geq 0$. These functions are continuous, and their derivatives exist up to and including the nth order and are continuous as well. In this TR either the real plane $\Re^2$ or a bounded subset of this plane is assumed to be the definition domain Ω. Accordingly often we refrain from stating the definition domain. Furthermore only the sets C^1, or C^2 are relevant in this TR. Functions of theses sets are called C^1-continuous respectively C^2-continuous surface functions.

A surface function $u = u(x, y)$ is also characterized by the validity or invalidity of the *integrability condition*

$$\frac{\partial^2 u(x,y)}{\partial x \partial y} = \frac{\partial^2 u(x,y)}{\partial y \partial x} \tag{28}$$

for all $(x, y) \in \Omega$. As a special corollary from Frobenius' theorem in mathematical analysis it follows that the validity of this condition $u_{xy} = u_{yx}$ is "approximately equivalent" to C^2-continuity (see [Klette et. al 1998]).

Function $u = u(x, y)$ is an *antiderivative of a vector field*

$$\mathbf{w}(x,y) = (p(x,y), q(x,y))$$

over a domain Ω if

$$p(x,y) = \frac{\partial u}{\partial x}(x,y) = u_x(x,y) \text{ and } q(x,y) = \frac{\partial u}{\partial y}(x,y) = u_y(x,y), \tag{29}$$

hold, for all $(x, y) \in \Omega$. Mathematical analysis offers (in principle) ways to calculate such an antiderivative. For example, the *integration of vector fields* can be based on arbitrarily specified *integration paths*, i.e. on piecewise C^1-curves

$$\gamma : \quad [a,b] \rightarrow \Re^2, \gamma(t) = (\gamma_1(t), \gamma_2(t)) = (x(t), y(t)) \tag{30}$$

that lies inside the region Ω, with $a < b$, $\gamma(a) = (x_0, y_0)$, and $\gamma(b) = (\hat{x}, \hat{y})$. For such a curve it holds that

$$u(\hat{x}, \hat{y}) = u(x_0, y_0) + \int_\gamma p(x,y)\, dx + q(x,y)\, dy. \tag{31}$$

where the result at position $(\hat{x}, \hat{y})$ is independent from the integration path.

The *depth map* respectively the *height map*, and the *gradient map* are functions over the image grid $\{(x, y) : 1 \leq x \leq M \wedge 1 \leq y \leq N\}$. In the ideal case at each point (x, y) a depth map for surface function u states the *depth* $u(x, y)$

of those surface point that is projected into this image point. A height map is defined relatively to an assumed background plane (of height zero), which is parallel to the image plane. In the ideal case at each point (x, y) the height value is equal to the (scaled) height of those surface point that is projected into this image point. Height is measured with respect to the chosen background plane. A given depth or height map allows us to reconstruct object faces in 3D space within a subsequent computation step of a general back projection approach. In this TR we consider depth or height maps as the ultimative goal of *single-view shape recovery*.

Shading based shape recovery techniques normally provide gradient values for a discrete set of visible points on object surfaces. This requires a subsequent integration step to achieve (within possible limits) the specified ultimative goal of (relative) depth or height maps.

The general remarks about integration paths support *local integration techniques*: Assume a scan algorithm which passes through all image points of the image grid (e.g. known under names as meander scan, Hilbert scan, or Peano scan etc.). Starting with initial depth values this algorithm can be used to propagate depth values according to a local approximation rule (e.g. based on the 4-neighborhood) using the given gradient data. Such a calculation of relative depth values can be done within repeated scans (i.e. using different scan algorithms). Finally resulting depth values can be determined by averaging operations. Initial depth values have to be provided or assumed for the start positions of the different runs.

Several proposals follow this general scheme of local propagations (for a review see [Klette & Schlüns 1996]). A *global integration method*, based on results of the paper [Frankot & Chellappa 1988] and presented in [Klette et. al 1998], leads practically to considerably better results for the task of calculating depth from gradients. The solution calculated by this *Frankot-Chellappa algorithm* is optimal in the sense of the quadratic error function between ideal and given gradient values. It only provides a relative height function up to an additive constant. See Fig. 10 for an example of a reconstructed surface.

3 Three Light Sources

This section discusses 3S PSM where it is assumed that no motion occurs inside the system consisting of the object, the light sources, and the sensor. Therefore, three irradiances (an irradiance triplet) can be assigned to every object point that is projected into the image plane. It is assumed that all irradiances are positive which means that shadows are excluded from the analysis. The smaller the angle between the illumination directions, the more object portions are covered simultaneously by all light sources. On the other hand, with smaller angles the sensitivity with respect to noise in the measurements of the irradiances during the image acquisition increases. The same holds for the sensitivity with respect to the inaccurate estimation of other fixed parameters, for example the illumination directions. Thus, no optimal choice of illumination directions exists for

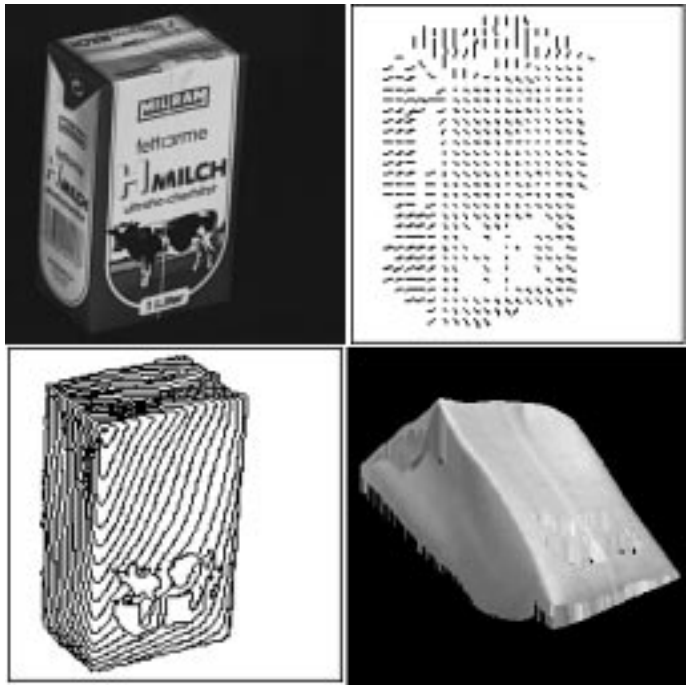

Figure 10: Top left: object. Top right: reconstructed gradient map using 3S PSM. Below: reconstruction results using the Frankot-Chellappa algorithm. Left: contour plot. Right: shaded surface with Lambertian texture for the lighting direction $\mathbf{s} = (0, 0, -1)$.

3S methods.

3.1 Albedo Dependent Analysis

We begin our discussion of shape recovery with the assumption of a Lambertian surface. The shape of a smooth genuine Lambertian surface with uniform albedo can be uniquely determined by 3S PSM, see [Horn 1986] or [Kozera 1991].

Three irradiance values are measured for any visible surface point where each value corresponds to the case that exactly one of the light sources was switched on. We assume a Gaussian sphere representation of the reflectance maps, i.e. each measured irradiance corresponds to a circle on the sphere representing all possible unity normals at the given surface point. This requires the assumption that for all three light sources the products $E_0 \cdot \rho$ of the light source irradiances and the albedo are known. On the Gaussian sphere the true orientation at the given surface point is represented by the intersection point of all these three circles on the Gaussian sphere (assuming non-coplanar light source orientations).

If the three illumination directions are not coplanar and the three image

irradiances are consistent with each other, then 3S PSM leads to a unique solution. The orientation of a point on a Lambertian surface can be recovered uniquely with three image irradiances independent of the neighborhood of the considered image point. We do not have to introduce smoothness assumptions or integrability constraints. The reconstruction of the surface orientations is carried out point-locally by analyzing irradiance triplets. But note that so far this is the ideal case in theory.

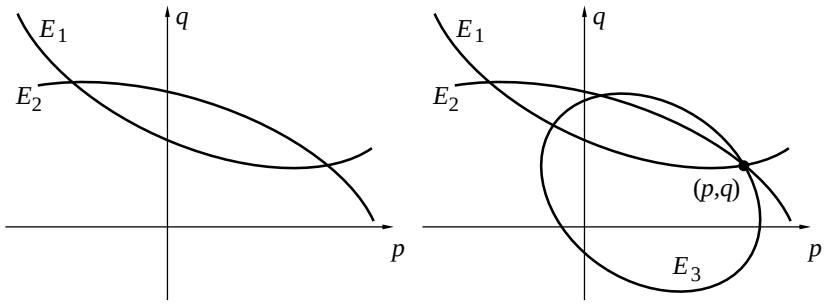

Figure 11: Isoirradiance curves of 2S (left) and 3S (right) PSM.

The pair of gradients of an irradiance pair is given by the intersection of two conic sections in the gradient space for a Lambertian surface. The left picture in Fig. 11 illustrates the intersection of two conic sections. When an additional light source is introduced which generates the image irradiance E_3 then the three conic sections intersect at a unique point. The intersection (p, q) in gradient space represents the desired orientation.

However, when the irradiances are measured for a real surface point, then basically there never exists a unique intersection due to noise and other errors. But even in this case two gradients would exist for each consistent pair of irradiances. If three consistent irradiance pairs are used to calculate the solution pairs, then six intersections occur. Three of the six intersections should represent orientations which point approximately into the same direction like the sought-after surface normal $\mathbf{n} = (p, q, -1)$. Finally not the gradients themselves but the orientations should be compared to determine an approximate orientation.

Furthermore, the recovery of the solution can also be achieved without explicitly calculating the solution candidates, simply by generating the intersection curves non-analytically. For this approach the reflectance maps are represented as image matrices. For this purpose at first a generation of the discrete reflectance maps (for all three light sources) can be performed. Using a calibration object has the advantage that neither the illumination directions nor the products $E_{0i}\rho$ have to be known. Then the selection of the orientations can be carried out through simple threshold segmentations of the reflectance maps. The three irradiances measured in the image are taken to specify the

thresholds. The segmentation result consists of three regions which represent the orientations that are consistent with the image irradiances. Finally, the binarized reflectance maps are intersected (binary AND operation). The centroid of the resulting region can be used to represent approximately the orientation at the considered image point. Note that the stereographic projection is a more convenient two-dimensional representation of the orientations since it causes less distortions. The width W of the segmentation interval $[E_i - W/2,\ E_i + W/2]$, with $i = 1, 2, 3$, can be adapted to the noise level in the image acquisition system and to expected variations in the albedo.

This described *threshold segmentation for 3S PSM* has the advantage that it is easily applicable to surfaces which have no Lambertian reflection properties since we do not have to solve a system of nonlinear equations. For reflectance maps that are synthetically generated and parameterized by a set of real parameters ambiguous solutions can easily be detected for a certain accuracy without a uniqueness proof. If the reflectance maps are generated by using a calibration object, then we do not have to determine the reflection parameters, i.e. the surface roughness and the ratio of the diffuse and the specular reflection component.

For a *look-up table solution to 3S PSM* note that an irradiance triplet that is measured in the images can be regarded as a point in a Cartesian coordinate system $E_1E_2E_3$ where each of the three axes (irradiance axis) represents the image irradiances of one light source. A surface orientation is uniquely assigned to every possible irradiance triplet, thus the generation of a three-dimensional look-up table is possible. The generation of the look-up table can be carried out in two different ways. If the illumination directions and irradiances of the light sources are known, then the look-up table can be built by applying explicit equations. Besides, a calibration object can be employed for the generation. Again it is of advantage that the directions and irradiances of the light sources as well as the reflection parameters do not have to be known explicitly. A surface orientation is determined by looking up the entry which corresponds to the measured irradiance triplet. The look-up table entry contains either a two-dimensional representation of the surface orientation or it is empty. If the image irradiances are digitized with 8-bit accuracy and the surface orientations are encoded with 2×4 Bytes, then the look-up table needs 128MB (!) of memory. Figure 12 illustrates two different views of a look-up table for a real sphere showing Lambertian reflection characteristics. The estimated illumination directions for the sphere are

$$\mathbf{s}_1 = (-0.312, -0.231, -1), \mathbf{s}_2 = (0.049, 0.304, -1), \text{and} \mathbf{s}_3 = (0.411, -0.236, -1).$$

The estimated ratios of the light source irradiances are $1.0 : 1.022 : 0.772$. A total number of 41717 triplets with positive 8-bit irradiances were measured on the sphere having a radius of 123 pixels. For the sake of clarity the illustrations only display 1303 irradiance triplets. Figure 12 on the right shows an orthographic projection of the look-up table.

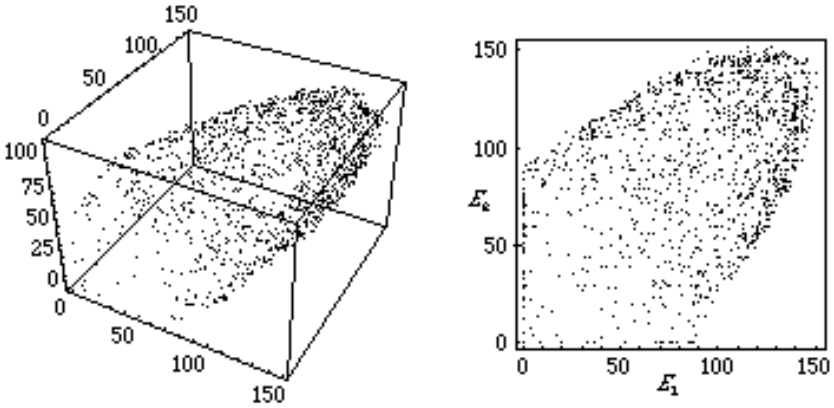

Figure 12: Left: the three-dimensional oblique view of a real look-up table in a coordinate system which is spanned by three irradiances originating from three different light sources. Right: orthogonal projection along the irradiance axis E_3.

It can easily be seen that the irradiances describe an ellipsoidal surface. In this example, the density of the look-up table is only approximately 3% with respect to the number of its entries. It can be shown that in the ideal case this point distribution describes in fact the surface of an ellipsoid [Woodham 1994]. The center of this ellipsoid is located at the origin of the $E_1E_2E_3$ coordinate system. The ellipsoid is restricted to the first octant of the coordinate system because only positive irradiances make sense. Each irradiance restricts the other two irradiance values to an ellipse in the $E_1E_2E_3$ space. Hence a unique solution is found by intersecting the three orthogonal ellipses.

The lengths of the three semiaxes of the ellipsoid are proportional to the albedo of the surface material. Moreover, the orientation of the ellipsoid is albedo independent and determined by the three illumination directions. Every ray in the $E_1E_2E_3$ space passing through the origin represents a unique orientation. From the mentioned properties it follows that the look-up table can be made albedo independent by propagating each entry along a ray. Thus, a valid surface orientation is assigned to every look-up table entry.

3.2 Albedo Independent Analysis

In the following it will be assumed that the albedo ρ stays unknown. At first we note that a pair of irradiances constrains the gradients of a Lambertian surface with unknown albedo to a straight line in gradient space, see [Lee & Rosenfeld 1984]. Under parallel illumination the two image irradiance equations of a Lambertian surface can be represented as

$$E_1 = E_{01}\rho\frac{\mathbf{n}^T\mathbf{s}_1}{\|\mathbf{n}\| \cdot \|\mathbf{s}_1\|} \text{ and } E_2 = E_{02}\rho\frac{\mathbf{n}^T\mathbf{s}_2}{\|\mathbf{n}\| \cdot \|\mathbf{s}_2\|} \tag{32}$$

resulting in the equation

$$\rho \cdot \mathbf{n}^T(E_{01} \cdot E_2 \|\mathbf{s}_2\| \mathbf{s}_1 - E_{02} \cdot E_1 \|\mathbf{s}_1\| \mathbf{s}_2) = 0, \tag{33}$$

which can be interpreted as a scaled scalar product. If $\rho \neq 0$, then the albedo can be eliminated from the equation which leads to albedo independence. By collecting the known quantities in $E_{0a,b} = E_{0a} \cdot E_b \|\mathbf{s}_b\|$ the equation can be represented as the simplified scalar product

$$\mathbf{n}^T(E_{01,2} \cdot \mathbf{s}_1 - E_{02,1} \cdot \mathbf{s}_2) = 0 \tag{34}$$

The representation

$$\mathbf{n}^T(\mathbf{s}_{1,2} - \mathbf{s}_{2,1}) = 0, \text{ with } \mathbf{s}_{a,b} = E_{0a,b} \cdot \mathbf{s}_a = E_{0a} \cdot E_b \|\mathbf{s}_b\| \mathbf{s}_a \tag{35}$$

is even more compact. The vector difference $\mathbf{s}_{1,2} - \mathbf{s}_{2,1}$ consists of known quantities and lies in the symmetry plane defined by the illumination directions $\mathbf{s}_1$ and $\mathbf{s}_2$. For a given illumination geometry the variables of the vector difference $\mathbf{s}_{1,2} - \mathbf{s}_{2,1}$ are just the two image irradiances E_1 and E_2. The vector $\mathbf{s}_1 \times \mathbf{s}_2$ is perpendicular to the set of vectors defined by $\mathbf{s}_{1,2} - \mathbf{s}_{2,1}$. The solutions of the above equation are vectors $\mathbf{n}$, for which the scalar product becomes zero. From this it follows that all those vectors $\mathbf{n}$ satisfy the equation which are oriented orthogonal to the vector difference $\mathbf{s}_{1,2} - \mathbf{s}_{2,1}$. The gradients of the possible vector differences $\mathbf{s}_{1,2} - \mathbf{s}_{2,1}$ lie in the gradient space on a determinable straight line h which is constant for a given illumination geometry. The straight line h is the line which is dual to the gradient $(p_s, q_s) = (p(\mathbf{s}_1 \times \mathbf{s}_2), q(\mathbf{s}_1 \times \mathbf{s}_2))$. A unique point on h is assigned to each irradiance pair (E_1, E_2). From the relationship

$$\mathbf{n}^T(\mathbf{s}_{1,2} - \mathbf{s}_{2,1}) = 0 \tag{36}$$

it follows that each gradient on the straight line h has a dual straight line k which represents the possible solutions $\mathbf{n}$ of equation (36).

The straight line h can be described explicitly by the equation

$$q_h = h(p_h) = -\frac{p_s}{q_s} \cdot p_h - \frac{1}{q_s}. \tag{37}$$

The set of straight lines generated by the straight line h can be represented explicitly by

$$q_k = k(p_k) = \frac{q_s}{1 + p_s \cdot p_h} \cdot (1 + p_h \cdot p_k). \tag{38}$$

The variable p_h itself depends on the measured image irradiance pair (E_1, E_2) and can be calculated by

$$p_h = p(\mathbf{w}) \ , \ \text{with} \ \ \mathbf{w} = E_{01} \cdot E_2 \, \|\mathbf{s}_2\| \, \mathbf{s}_1 - E_{02} \cdot E_1 \, \|\mathbf{s}_1\| \, \mathbf{s}_2 . \tag{39}$$

Thus, all gradients which are consistent with any arbitrary irradiance pair can be calculated by using equation (36). It can be shown that the gradient (p_s, q_s) lies on the straight line k. The albedo ρ can be found for every gradient by substituting a solution into any of the two image irradiance equations.

Similar equations to equation (36) can be formulated for the irradiance pairs (E_1, E_3) and (E_2, E_3). For the pair (E_1, E_3) the equation

$$\mathbf{n}^T (E_{01} \cdot E_3 \, \|\mathbf{s}_3\| \, \mathbf{s}_1 - E_{03} \cdot E_1 \, \|\mathbf{s}_1\| \, \mathbf{s}_3) = 0 \tag{40}$$

arises, which can be combined with the equation for the image irradiance pair (E_1, E_2). The terms in parentheses are vectors which are orthogonal to the desired surface orientation $\mathbf{n}$. After calculating the vector product

$$\mathbf{w} = (E_{01} \cdot E_2 \, \|\mathbf{s}_2\| \, \mathbf{s}_1 - E_{02} \cdot E_1 \, \|\mathbf{s}_1\| \, \mathbf{s}_2) \times (E_{01} \cdot E_3 \, \|\mathbf{s}_3\| \, \mathbf{s}_1 - E_{03} \cdot E_1 \, \|\mathbf{s}_1\| \, \mathbf{s}_3) \tag{41}$$

a vector results which is collinear to the surface normal $\mathbf{n}$. Therefore, $\mathbf{n} = \mathbf{s} \cdot \mathbf{w}$. The scaling factor s must have such a sign that the surface normal $\mathbf{n}$ obtains a negative z-component. Besides the surface normal the albedo can be point-locally recovered by substituting the normalized vector $\mathbf{n}^\circ$ into one of the three image irradiance equations. When the equation is divided by one of the three irradiances of the light sources, for example by E_{03}, then the direction of the calculated vector

$$\mathbf{w}* = (\frac{E_{01}}{E_{03}} \cdot E_2 \, \|\mathbf{s}_2\| \, \mathbf{s}_1 - \frac{E_{02}}{E_{03}} \cdot E_1 \, \|\mathbf{s}_1\| \, \mathbf{s}_2) \times (\frac{E_{01}}{E_{03}} \cdot E_3 \, \|\mathbf{s}_3\| \, \mathbf{s}_1 - E_1 \, \|\mathbf{s}_1\| \, \mathbf{s}_3) \tag{42}$$

does not change with respect to $\mathbf{w}$. This property is helpful for the realization of an albedo independent photometric stereo method since it means that only the ratios of the irradiances of the light sources have to be known. This leads to a different scaling of the albedo value.
Figure 13 shows three input images of a synthetic Mozart statue for the described 3S photometric stereo method. The images were generated by using Lambertian reflectance maps. A light source set-up having the *slant angles*

Figure 13: Image triplet of a synthetic Mozart statue for 3S photometric stereo. In the text the indices 1, 2, and 3 are assigned to the images from left to right.

$$\sigma(\mathbf{s}_1) = \sigma(\mathbf{s}_2) = \sigma(\mathbf{s}_3) = 20^\circ$$

and the *tilt angles*

$$\theta(\mathbf{s}_1) = 90^\circ,\ \theta(\mathbf{s}_2) = -150^\circ,\ \theta(\mathbf{s}_3) = -30^\circ$$

were chosen for rendering. Relatively small slant angles for the illumination directions guarantee that no strong self-shadows arise. The ratios of the irradiance values E_{0i} of the light sources are equal to one.

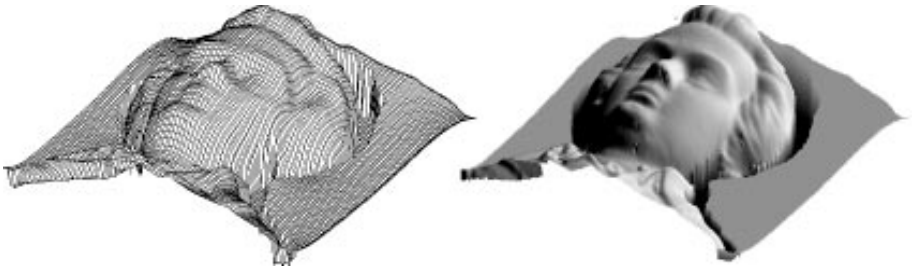

Figure 14: Surface reconstruction results. Left: grid representation. Right: texture mapping.

Figure 14 illustrates the shape recovery results for the Mozart statue. The integration of the height map was carried out using the Frankot-Chellappa algorithm, see Section 2.3. The left picture of Fig. 14 shows a grid representation of the reconstruction. Since detail information gets lost in this representation the right hand picture presents the same surface by using texture mapping. The texture image was calculated from the recovered surface normals by using a Lambertian reflectance map with the illumination direction $\mathbf{s} = (1, 1, -1)$.

The image triplet of a real hand shown in Fig. 15 is an example of an object with a non-constant albedo (different blood circulation). The ratios of the light

source irradiances were estimated as $1.0 : 0.638 : 0.640$. Estimations for the illumination directions of the three hand images are

$\mathbf{s}_1 = (-0.370, -0.028, -1)$, $\mathbf{s}_2 = (0.044, 0.472, -1)$, and $\mathbf{s}_3 = (0.420, 0.043, -1)$.

The 3D plots presented in Fig. 16 show that a good surface reconstruction is possible by using 3S photometric stereo. Artifacts can occur when the hand is not entirely still and when the specular reflection component (caused by the transpiration) is not taken into account by the reflection model. In the right picture of Fig. 16 the first input image is mapped onto the 3D reconstruction.

Figure 15: An image triplet of a real hand used as input for a 3S photometric stereo method. The images 2 and 3 were brightened for visualization purposes where the indices 1, 2, and 3 are assigned to the images from left to right.

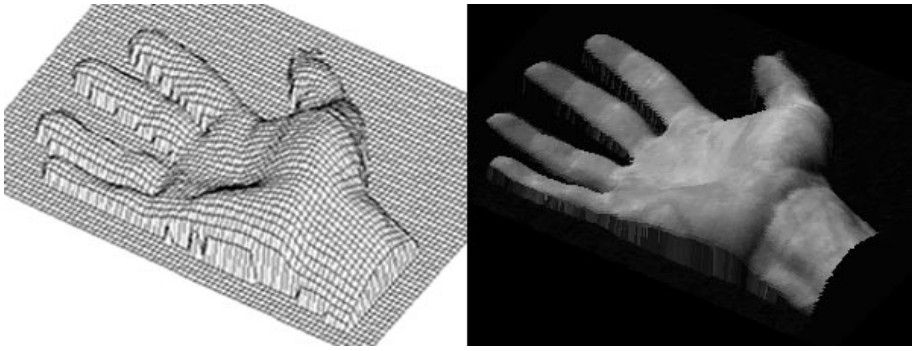

Figure 16: Surface reconstruction results. Left: grid representation. Right: first input image was chosen for texture mapping.

4 Two Light Sources

A more complex task is given if only two light sources shall be used to accomplish the task of unique surface recovery. The illumination directions $\mathbf{p}$ and $\mathbf{q}$ of

the two light sources are assumed to be not collinear. In order to prevent an interference of the irradiances of the two light sources, the two pictures have to be taken consecutively. The object and the camera have a fixed position and orientation. Thus, an irradiance pair (E_1, E_2) is assigned to each image point and the corresponding surface point for 2S PSM.

4.1 Albedo Dependent Analysis

This section focuses on fundamentals of situations when the shape of a smooth Lambertian surface is uniquely determined by a pair of images. More applied results for 2S PSM can be found in [Klette et. al 1998]. At first we discuss gradient computation and then we analyze the corresponding uniqueness and existence problems. For more detailed texts an interested reader is referred to [Kozera 1991, Kozera 1992] or [Onn & Bruckstein 1990]. The second stage of the shape recovery process involves gradient integration as already discussed in Section 2.

Suppose that a genuine Lambertian surface represented by the graph of a function u of class C^1 defined over a domain $\Omega = \Omega_1 \cap \Omega_2$, is illuminated from two linearly independent directions, $\mathbf{p} = (p_1, p_2, p_3)$ and $\mathbf{q} = (q_1, q_2, q_3)$. The captured images are E_1 and E_2, respectively. We assume that the albedo $\rho(x, y)$ is constant over the entire domain Ω with $\rho(x, y) \equiv c$ and $0 < c \leq 1$. Note that $\langle \mathbf{p}|\mathbf{q} \rangle$ is the dot product of both vectors. We then have the following (see [Kozera 1991] and [Onn & Bruckstein 1990]):

Theorem 2 *The first derivatives u_x and u_y of function u can be expressed in terms of E_1, E_2, $\mathbf{p}$, and $\mathbf{q}$, where $\|\mathbf{p}\| = \|\mathbf{q}\| = 1$, in the following form $u_x = e_1/e_3$ and $u_y = e_2/e_3$, where*

$$\begin{aligned} e_1 &= (q_1\langle \mathbf{p}|\mathbf{q} \rangle - p_1)E_1 + (p_1\langle \mathbf{p}|\mathbf{q} \rangle - q_1)E_2 + (p_3q_2 - p_2q_3)\varepsilon\sqrt{\Lambda}, \\ e_2 &= (q_2\langle \mathbf{p}|\mathbf{q} \rangle - p_2)E_1 + (p_2\langle \mathbf{p}|\mathbf{q} \rangle - q_2)E_2 + (p_1q_3 - p_3q_1)\varepsilon\sqrt{\Lambda}, \\ e_3 &= (p_3 - q_3\langle \mathbf{p}|\mathbf{q} \rangle)E_1 + (q_3 - p_3\langle \mathbf{p}|\mathbf{q} \rangle)E_2 + (p_1q_2 - p_2q_1)\varepsilon\sqrt{\Lambda}, \end{aligned} \tag{43}$$

and where

$$\Lambda = \Lambda(x, y) = \big[1 - E_1^2(x, y) - E_2^2(x, y)\big] - \langle \mathbf{p}|\mathbf{q} \rangle \big[\langle \mathbf{p}|\mathbf{q} \rangle - 2E_1(x, y)E_2(x, y)\big],$$

and $\varepsilon = \varepsilon(x, y)$ is a function taking values ± 1 so that $f(x, y) = \varepsilon(x, y)\sqrt{\Lambda(x, y)}$ is a continuous function.

The Case when $\Lambda > 0$: When Λ is positive over Ω, the function ε appearing in (43) must take one of the values 1 or -1 since the gradient (u_x, u_y) has to be a continuous function. As an immediate consequence, Theorem 2 implies that there exist at most two C^2/C^1 solutions to the system (2).

The next theorem formulates necessary and sufficient conditions for the existence of exactly two solutions of class C^2 (and so of class C^1) to the system (2) (see also [Kozera 1991] and [Onn & Bruckstein 1990]).

Theorem 3 *Let E_1 and E_2 be functions of class C^1 over a simply connected region Ω of $\Re^2$ with values in $(0,1]$ and let e_1, e_2, and e_3 be defined by (43). Suppose that $\Lambda > 0$ on Ω and that, for each choice of sign, $\sigma^{\pm} = (p_3 - q_3\langle \mathbf{p}|\mathbf{q}\rangle)E_1 + (q_3 - p_3\langle \mathbf{p}|\mathbf{q}\rangle)E_2 \pm (p_1 q_2 - p_2 q_1)\sqrt{\Lambda}$ does not vanish over Ω. Then*

$$(e_1/e_3)_y = (e_2/e_3)_x \tag{44}$$

is a necessary and sufficient condition for the existence of exactly two solutions of class C^2 to (2), for each choice of sign.

Consequently, if both vector fields (u_x^+, u_y^+) where $\varepsilon(x,y) \equiv 1$, and (u_x^-, u_y^-) where $\varepsilon(x,y) \equiv -1$ are integrable (see condition (44)) then there exist exactly two C^2 class solutions to problem (2) over Ω.

Now we analyse the meaning of condition (44) for images E_1 and E_2 generated by a C^2 Lambertian surface, that is, when (2) is satisfied for a certain function u of class C^2. We have the following (see also [Kozera 1992] and [Onn & Bruckstein 1990]):

Theorem 4 *Let $\mathbf{p} = (0,0,-1)$ and $\mathbf{q} = (q_1, q_2, q_3)$ be such that $q_1^2 + q_2^2 > 0$ and $\|\mathbf{q}\| = 1$, and let u be a function of class C^2 on a simply connected open subset Ω of $\Re^2$. Suppose that functions E_1 and E_2 are given by (2). Suppose, moreover, that $\Lambda > 0$ over Ω. In order that there exist a solution of class C^2 to (2) different from u, it is necessary and sufficient that u satisfies*

$$q_1 q_2 (u_{yy} - u_{xx}) + (q_1^2 - q_2^2) u_{xy} = 0. \tag{45}$$

As the equation (45) is generically not satisfied by function u, a C^2 class uniqueness, in the case when $\Lambda > 0$ over Ω, is therefore in most cases assured. In other words, the integrability condition (45) disambiguates surface reconstruction for two image patterns and essentially ascertains *a generic uniqueness* for 2S PSM.

In connection with the above theorem a natural question arises about possible analytic and geometric relationship between these two solutions (if both exist). Clearly, each of them has to satisfy additional constraint imposed by (45). A *standard method of characteristics*, see the classical theory of the second-order partial differential equations [John 1971], applied to (45) yields (see [Kozera 1991]):

Theorem 5 *Suppose that $q_1^2 + q_2^2 > 0$. Any solution u of class C^2 to (45) over an open convex region Ω is given by*

$$u(x,y) = \begin{cases} \phi(q_1 x + q_2 y) + \psi(q_1 x - q_2 y) & if \quad q_1 q_2 \neq 0, \\ \phi(x) + \psi(y) & if \quad q_1 q_2 = 0, \end{cases} \tag{46}$$

for some functions ϕ and ψ of class C^2. Conversely, for any functions ϕ and ψ of class C^2, the above formula defines a solution of class C^2 to (45). In addition, if a C^2 class function u satisfying (45) is determined, then the corresponding functions ϕ and ψ can be found by using the following formulae:

$$\phi(x) = \begin{cases} u(q_1 x/(q_1^2 + q_2^2), q_2 x/(q_1^2 + q_2^2)) - c & if \quad q_1 q_2 \neq 0, \\ u(x,0) - c & if \quad q_1 q_2 = 0, \end{cases} \tag{47}$$

$$\psi(x) = \begin{cases} u(-q_2 x/(q_1^2+q_2^2), q_1 x/(q_1^2+q_2^2)) + c & if \quad q_1 q_2 \neq 0, \\ u(0,x) + c & if \quad q_1 q_2 = 0, \end{cases} \tag{48}$$

where c is an arbitrary constant.

The last theorem implies that, if there exist two C^2 class solutions to (45) (which is a rare case) then each of them can be decomposed as a sum of two single-variable C^2 class functions. A natural question arises about the relationship between pairs (ϕ_u, ψ_u) and (ϕ_v, ψ_v). This is answered by the following (see [Kozera 1992]):

Theorem 6 *Let $\mathbf{p} = (0,0,-1)$ and $\mathbf{q} = (q_1, q_2, q_3)$ be such that $q_1^2 + q_2^2 > 0$ and $\|\mathbf{q}\| = 1$. Let u be a function of class C^2 defined over and open convex region Ω, satisfying (2) and*

$$u(x,y) = \begin{cases} \phi(q_1 x + q_2 y) + \psi(q_1 x - q_2 y) & if \quad q_1 q_2 \neq 0, \\ \phi(x) + \psi(y) & if \quad q_1 q_2 = 0, \end{cases}$$

for some functions ϕ and ψ of class C^2. Then the second solution v to (2) of class C^2 can be expressed in the form:

$$v(x,y) = \begin{cases} \phi(q_1 x + q_2 y) - \psi(q_1 x - q_2 y) & if \quad q_1 q_2 \neq 0, \\ -\phi(x) + \psi(y) & if \quad q_1 = 0, \\ \phi(x) - \psi(y) & if \quad q_2 = 0. \end{cases}$$

The last two theorems determine *analytic representations* of two C^2 class solutions as well as establish the corresponding relationship between these representations. Furthermore, one can derive now *two alternative schemes* for finding those two solutions (if both exist). First, as indicated in Theorem 2 and 3 one can recover both functions u and v by calculating the corresponding contour integrals. However, only one contour integration is in fact necessary. Having found the first solution u, we can apply Theorem 5 and decompose u in terms of a pair of C^2 class functions (ϕ, ψ). Finally, Theorem 6 renders the second solution v, represented uniquely in terms of a pair of functions (ϕ, ψ).

In addition, *a geometric relationship* between the graphs of two solutions u and v can also be now established. Namely, as easily verified, the Gaussian curvature $K_u(x,y)$ of the graph of function u calculated at point $(x, y, u(x,y))$, and the Gaussian curvature $K_v(x,y)$ of the graph of function v calculated at point $(x, y, v(x,y))$ satisfy $K_u(x,y) = -K_v(x,y)$.

The immediate consequence of this fact is that, there is no $\pm u + c$ ambiguity in 2S PSM when both Λ and the Gaussian curvature of at least one solution do not vanish. Such a symmetry is characteristic for the single-image shape recovery when a point light-source is positioned overhead. However, one can expect non-uniqueness (in two point light-source photometric stereo) resulting from replacing u by $-u + c$ for the graphs with zero Gaussiam curvature. Note also that, if an admissible class of shapes contains only *convex/concave surfaces* consisting exclusively of elliptic points the second solution (if it exists) consists exclusively of *hyperbolic points*. Such a theoretical solution is considered not

physically plausible as being *a priori* excluded from an admissible class of surfaces. Consequently, any restriction of class of admissible solutions, might also disambiguate a possible case of non-uniqueness in 2S PSM.

Example 2 Let $\mathbf{p} = (0, 0, -1)$ and $\mathbf{q} = (1/\sqrt{3}, 1/\sqrt{3}, -1/\sqrt{3})$. Let $E_1(x, y) = (x^2 + y^2 + 1)^{-1/2}$ and $E_2(x, y) = (x + y + 1)\big[3(x^2 + y^2 + 1)\big]^{-1/2}$. Consider the corresponding two image irradiance equations for 2S PSM:

$$\begin{aligned} \frac{1}{\sqrt{u_x^2 + u_y^2 + 1}} &= \frac{1}{\sqrt{x^2 + y^2 + 1}}, \\ \frac{u_x + u_y + 1}{\sqrt{3}\sqrt{u_x^2 + u_y^2 + 1}} &= \frac{x + y + 1}{\sqrt{3}\sqrt{x^2 + y^2 + 1}} \end{aligned} \tag{49}$$

defined over $\Sigma = \{(x, y) \in \Re^2 : x + y + 1 \geq 0,\ x < y\}$. An easy inspection shows that Λ vanishes only along the line $x = y$ and thus Λ is positive over Σ. Applying Theorems 2 and 3 yields that both vector fields $(u_x^+, u_y^+) = (y, x)$ and $(u_x^-, u_y^-) = (x, y)$ are C^2 integrable. Moreover, the corresponding C^2/C^1 class solutions to (49), defined over Σ, are given up to a constant as $u^+(x, y) = xy$ and $u^-(x, y) = \frac{1}{2}(x^2 + y^2)$. Alternatively, we can first integrate one of the vector fields, say (u_x^+, u_y^+) and verify that u^+ satisfies (45). Hence the second vector field (u_x^-, u_y^-) is also C^2 integrable. By (46), the function $u^+(x, y) = \phi(1/\sqrt{3}(x + y)) + \psi(1/\sqrt{3}(y - x))$. Furthermore, formulae (47) and (48) yield $\phi(x) = u^+((\sqrt{3}x/2), (\sqrt{3}x/2)) - c = (3/4)x^2 - c$ and $\psi(x) = u^+(-(\sqrt{3}x/2), (\sqrt{3}x/2)) + c = -(3/4)x^2 + c$. Using Theorem 6 results in $u^-(x, y) = \phi(1/\sqrt{3}(x+y)) - \psi(1/\sqrt{3}(y-x)) = (x^2+y^2)/2$, which obviously coincides with the second solution, already determined by using a standard contour gradient integration method. Observe that u^- also satisfies (45). Note, moreover, that the graph of u^+ consists exclusively of hyperbolic points with negative Gaussian curvature $K_{u^+}(x, y) = -(1+x^2+y^2)^{-2}$, whereas the graph of u^- consists exclusively of elliptic points with positive Gaussian curvature $K_{u^-}(x, y) = (1 + x^2 + y^2)^{-2}$. Hence, the equation $K_u(x, y, u(x, y)) = -K_v(x, y, v(x, y))$ is clearly also fulfilled. The reconstructed surfaces coincide with the Lambertian paraboloid and hyperboloid, respectively.

The Case when $\Lambda \equiv 0$: We consider the case when Λ introduced in Theorem 2 vanishes, for given E_1 and E_2 defined (captured) over some domain Ω.

An immediate consequence of Theorem 2 is that there is at most one C^2/C^1 class solution to the system (2). The next theorem formulates a necessary and sufficient condition for existence of exactly one solution u of class C^2 to the system (2) (see [Kozera 1991]).

Theorem 7 *Let E_1 and E_2 be functions of class C^1 over a simply connected region Ω of $\Re^2$ with values in $(0, 1]$. Suppose that $\Lambda \equiv 0$ on Ω and that $\sigma = (p_3 - q_3\langle \mathbf{p}|\mathbf{q}\rangle)E_1 + (q_3 - p_3\langle \mathbf{p}|\mathbf{q}\rangle)E_2$ does not vanish over Ω. Then a necessary*

and sufficient condition for the existence of exactly one class C^2 solution u of (2) *is* $(g_1/g_3)_y = (g_2/g_3)_x$, *where*

$$\begin{aligned} g_1 &= (q_1\langle \mathbf{p}|\mathbf{q}\rangle - p_1)E_1 + (p_1\langle \mathbf{p}|\mathbf{q}\rangle - q_1)E_2, \\ g_2 &= (q_2\langle \mathbf{p}|\mathbf{q}\rangle - p_2)E_1 + (p_2\langle \mathbf{p}|\mathbf{q}\rangle - q_2)E_2, \\ g_3 &= (p_3 - q_3\langle \mathbf{p}|\mathbf{q}\rangle)E_1 + (q_3 - p_3\langle \mathbf{p}|\mathbf{q}\rangle)E_2. \end{aligned}$$

Furthermore, in case of Λ vanishing over Ω, it can be shown that the graph of u constitutes *a developable surface of cylindrical type* and that vectors, $\mathbf{n} = (u_x, u_y, -1)$, $\mathbf{p}$, and $\mathbf{q}$ are co-planar, for each $(x, y) \in \Omega$. For a more detailed analysis an interested reader is referred to [Kozera 1992].

We close this subsection with an example highlighting another important aspect appearing in 2S PSM. As it turns out, the uniqueness problem is not a mere function of an unknown surface but also depends on the mutual position of vectors $\mathbf{n} = (u_x, u_y, -1)$, $\mathbf{p}$, and $\mathbf{q}$. This is explicitly illustrated in the following example:

Example 3 Let $\mathbf{q} = (q_1(q_1^2+q_2^2+1)^{-1/2}, q_2(q_1^2+q_2^2+1)^{-1/2}, -(q_1^2+q_2^2+1)^{-1/2})$ and $\mathbf{p} = (0, 0, -1)$, and let $E_1(x, y) = (a^2 + b^2 + 1)^{-1/2}$ and $E_2(x, y) = (aq_1 + bq_2+1)(a^2+b^2+1)^{-1/2}(q_1^2+q_2^2+1)^{-1/2}$. Assume that vectors $\mathbf{p}$ and $\mathbf{q}$ are linearly independent. Consider now the corresponding two image irradiance equations for 2S PSM:

$$\begin{aligned} \frac{1}{\sqrt{u_x^2 + u_y^2 + 1}} &= \frac{1}{\sqrt{a^2 + b^2 + 1}}, \\ \frac{q_1u_x + q_2u_y + 1}{\sqrt{q_1^2 + q_2^2 + 1}\sqrt{u_x^2 + u_y^2 + 1}} &= \frac{q_1a + q_2b + 1}{\sqrt{q_1^2 + q_2^2 + 1}\sqrt{a^2 + b^2 + 1}}. \end{aligned} \tag{50}$$

As straightforward calculation shows that Λ vanishes over Ω, if $aq_2 - bq_1 = 0$. The latter happens only and only if three vectors $\mathbf{n} = (u_x, u_y, -1)$, $\mathbf{p}$, and $\mathbf{q}$ are co-planar, i.e. when they are linearly dependent. Theorem 7 yields the existence of exactly one C^2/C^1 solution to (50) defined as $u(x, y) = ax+by+c$. If, in turn, $aq_2-bq_1 \neq 0$ (i.e. vectors $\mathbf{n}$, $\mathbf{p}$, and $\mathbf{q}$ are linearly independent) then Λ is positive over Ω. Thus, the Theorem 3 assures the existence of exactly two C^2/C^1 solutions: $u^+(x, y) = ax+by+c$ and $u^-(x, y) = Ax+By+c$, where $A = (a(q_1^2-q_2^2)+2bq_1q_2)/(q_1^2+q_2^2)$ and $B = (b(q_2^2-q_1^2)+2aq_1q_2)/(q_1^2+q_2^2)$. As expected, the condition (45) is satisfied by both u^+ and u^- and $K_{u^+}(x, y, u^+(x, y)) = -K_{u^-}(x, y, u^-(x, y)) = 0$. Note, finally, that each reconstructed surface coincides with a Lambertian plane.

The Case when $\Lambda \geq 0$: So far we have considered the cases in which Λ is either positive or vanishes over a given domain Ω. Now we shall treat the situation in which Λ is non-negative. Our analysis will not be complete as we shall confine ourselves to the specific case concerning the topology of the zero sets of Λ.

Namely, we assume that region $\Omega = D_1 \cup D_2 \cup \Gamma$, where subdomains D_1 and D_2, and a smooth curve Γ are mutually disjoint, Λ is positive over $D_1 \cup D_2$, and Λ vanishes over Γ. It can be verified that this special topological case is obeyed by most pairs of images and pairs of point light-source directions.

Assume that there exists at least one solution u of class C^2 to (2) and that the irradiance functions E_1, E_2 appearing in these equations are C^1 class over Ω. Suppose that the set $\{(x,y) \in \Omega : \Lambda = 0\}$ is a smooth curve Γ such that $\Omega \setminus \Gamma = D_1 \cup D_2$, where D_1 and D_2 are disjoint open subsets of Ω, on which, of course, Λ is positive. By Theorem 3, there exist at most two solutions (u_1^1, u_1^2) to (2) of class C^2 over D_1 and at most two solutions (u_2^1, u_2^2) to (2) of class C^2 over D_2, respectively. We do not exclude the possibility that $u_i^1 = u_i^2$ for either $i = 1$, or $i = 2$, or $i = 1$ and $i = 2$. Clearly, the restriction of u to D_i coincides with either u_i^1 or u_i^2 for $i = 1, 2$. Conversely, suppose that for some i and j with $i, j = 1, 2$ and some constant c the limits $\lim_{(x',y') \in D_1 \to (x,y) \in \Gamma} u_1^i(x',y') = \lim_{(x',y') \in D_2 \to (x,y) \in \Gamma} (u_2^j(x',y') + c) = g^{ij}(x,y)$ exist for each $(x,y) \in \Gamma$. Set

$$v_{ij}(x,y) = \begin{cases} u_1^i(x,y) & if (x,y) \in D_1, \\ g^{ij}(x,y) & if (x,y) \in \Gamma, \\ u_2^j(x,y) + c & if (x,y) \in D_2 \end{cases} \tag{51}$$

and suppose that for each $(x,y) \in \Gamma$ the function v_{ij} is of class C^2. Then v_{ij} is a class C^2 solution of (2) over Ω and in such a case we say that the functions u_1^i and u_2^j *bifurcate* along Γ in the C^2 class. It is clear that, up to a constant, one can define in this way at most four solutions of class C^2 to (2) over Ω.

The next result establishes necessary and sufficient conditions for such a bifurcation to take place (see [Kozera 1991]):

Theorem 8 *Let* $\mathbf{p} = (0, 0, -1)$ *and let* $\mathbf{q} = (q_1, q_2, q_3)$ *be such that* $q_1^2 + q_2^2 > 0$ *and* $\|\mathbf{q}\| = 1$. *For a pair of* C^1 *class functions* E_1 *and* E_2 *defining a system* (2), *suppose that the set* $\{(x,y) \in \Omega : \Lambda = 0\}$ *is a smooth curve* Γ *such that* $\Omega \setminus \Gamma = D_1 \cup D_2$, *where* D_1 *and* D_2 *are disjoint open subsets of* Ω. *Assume that there exist two different solutions of class* C^2 *to* (2) *over* D_1 *and two different solutions of class* C^2 *to* (2) *over* D_2, *respectively. Let* u *be a solution over* D_1 *and* v *be a solution over* D_2 *such that* $g(x,y) = \lim_{(x',y') \in D_1 \to (x,y) \in \Gamma} u(x',y')$ $= \lim_{(x',y') \in D_2 \to (x,y) \in \Gamma} (v(x',y') + c)$, *for some choice of constant* c. *Assume, moreover, that the triplet of functions* (u, v, g) *defines in* (51) *a* C^1 *class function* z *over* Ω. *If* $q_1^2 - q_2^2 \neq 0$, *then the function* z *is of class* C^2 *over* Ω *if and only if, for each* $(x,y) \in \Gamma$,

$$\lim_{(x',y') \in D_1 \to (x,y) \in \Gamma} u_{xx}(x',y') = \lim_{(x',y') \in D_2 \to (x,y) \in \Gamma} v_{xx}(x',y'),$$
$$\lim_{(x',y') \in D_1 \to (x,y) \in \Gamma} u_{yy}(x',y') = \lim_{(x',y') \in D_2 \to (x,y) \in \Gamma} v_{yy}(x',y').$$

If $q_1^2 - q_2^2 = 0$, *then the function* z *is of class* C^2 *over* Ω *if and only if, for each*

$(x,y) \in \Gamma$, *either*

$$\lim_{(x',y') \in D_1 \to (x,y) \in \Gamma} u_{xx}(x',y') = \lim_{(x',y') \in D_2 \to (x,y) \in \Gamma} v_{xx}(x',y'),$$
$$\lim_{(x',y') \in D_1 \to (x,y) \in \Gamma} u_{xy}(x',y') = \lim_{(x',y') \in D_2 \to (x,y) \in \Gamma} v_{xy}(x',y'),$$

or

$$\lim_{(x',y') \in D_1 \to (x,y) \in \Gamma} u_{yy}(x',y') = \lim_{(x',y') \in D_2 \to (x,y) \in \Gamma} v_{yy}(x',y'),$$
$$\lim_{(x',y') \in D_1 \to (x,y) \in \Gamma} u_{xy}(x',y') = \lim_{(x',y') \in D_2 \to (x,y) \in \Gamma} v_{xy}(x',y').$$

It should be emphasized that a similar result establishing sufficient conditions for C^1 class bifurcations can be derived. As shown in [Kozera 1991] such bifurcations are generically feasible. Furthermore, it can also be proved that, if there exist exactly two C^2 class solutions to (2), defined over D_1 and D_2, then only an even number of C^2 class bifurcations is possible. This combined with the case of having exactly one C^2 solution over D_1 and/or D_2 permits to have either zero, one, two, or four C^2 class solutions to (2), defined globally over Ω. Recall, however, that the existence of a unique solution of class C^2, over D_1 and D_2, is generically assured (see the subsection covering the case when $\Lambda > 0$). Therefore, a global generic uniqueness result for C^2 class functions, considered over Ω can also be ascertained.

An interested reader is referred to [Kozera 1992] for a more detailed discussion of this case. We present now an example in which a different number of C^2/C^1 class bifurcations appear in 2S PSM.

Example 4 *One bifurcation - a generic case*: Assume that $\mathbf{p} = (0,0,-1)$ and $\mathbf{q} = (q_1,q_2,q_3)$ are linearly independent and that $\|\mathbf{q}\| = 1$. It is easy to show that for the corresponding two images of a Lambertian hemisphere $u_h(x,y) = -\sqrt{1-x^2-y^2}$, function Λ vanishes along $\Gamma = \{(x,y) \in \Omega : q_2 x - q_1 y = 0\}$. Clearly, the curve Γ decomposes Ω into two disjoints subdomains D_1 and D_2, over which Λ is positive. As the condition (45) is not satisfied by u_h over both D_1 and D_2, Theorem 4 assures that there exists exactly one C^2 class solution over each D_1 and D_2 which is u_h. Thus, there can be maximum one C^2 class solution over Ω, subject to the existence of a successful C^2 class bifurcation along the curve Γ. As the hemisphere u_h constitutes a global C^2 class solution over Ω, the existence of at least one C^2 class bifurcation is therefore ascertained. Summing up, two images of a Lambertian hemisphere can be uniquely interpreted within the set of C^2 class functions.

Two bifurcations: Consider two image irradiance equations introduced in Example 3. Let Ω be a simply connected set containing the $D_1 = \{(x,y) \in \Omega : x < y\}$, $D_2 = \{(x,y) \in \Omega : x > y\}$, and $\Gamma = \{(x,y) \in \Omega : x = y\}$. As mentioned before Λ vanishes along Γ and, moreover, there exist exactly two C^2 class solutions to (49), over D_1 and D_2, defined as follows: $u^+(x,y) = xy$ and $u^-(x,y) = (x^2+y^2)/2$. An easy inspection shows that only two C^2 class bifurcations succeed. Namely, by using (51), formulae $u(x,y) = xy$ and

$v(x,y) = (x^2+y^2)/2$ yield two C^2 class functions defined globally over entire Ω. The remaining two other functions (introduced in (51))

$$w(x,y) = \begin{cases} xy & if(x,y) \in D_1, \\ x^2 & if(x,y) \in \Gamma, \\ (x^2+y^2)/2 & if(x,y) \in D_2 \end{cases}$$

$$z(x,y) = \begin{cases} (x^2+y^2)/2 & if(x,y) \in D_1, \\ x^2 & if(x,y) \in \Gamma, \\ xy & if(x,y) \in D_2 \end{cases}$$

are not of class C^2 along the line Γ. A simple verification shows, however, that both functions w and z are still C^1 class functions over Γ. Hence there exist exactly two (four) C^2 (C^1) class solutions to the problem (49) considered over entire Ω.

Four bifurcations: Let $\mathbf{p} = (0,0,-1)$ and $\mathbf{q} = (0,1/\sqrt{2},-1/\sqrt{2})$, and let $E_1(x,y) = (1+x^8)^{-1/2}$ and $E_2(x,y) = (2(1+x^8))^{-1/2}$ be defined over $\Omega = \Re^2$. A straightforward calculation shows that for the corresponding two image irradiance equations a function Λ vanishes only along the line $x = 0$, i.e. over the $y-$axis. Moreover, there exist, over both $D_1 = \{(x,y) \in \Re^2 : x > 0\}$ and $D_2 = \{(x,y) \in \Re^2 : x < 0\}$, exactly two C^2 class solutions: $u(x,y) = x^5/5$ and $v(x,y) = -x^5/5$. It is a matter of simple calculation to show that four functions: v_{11}, v_{12}, v_{21}, and v_{22} (defined with the aid of formula (51)) are of class C^2 over Γ. Therefore, there exist exactly four C^2 class solutions over entire Ω. Note that, if Ω does not contain $y-$axis, then there existonly two C^2 class solutions to the corresponding 2S PSM problem, namely u and v, and in this case there is no possibility of having bifurcations.

It is evident now, that bifurcations can either reduce or increase the number of global C^2/C^1 class solutions over the entire domain Ω. However, a reduction case, due to the condition (45), is generic. Note finally, that if none of the integrability conditions is fulfilled or none of the bifurcations succeeds, a pair of such *spurious images* cannot be generated by a genuine Lambertian surface, see [Kozera 1991].

4.2 Albedo Independent Analysis

As discussed for equation (39), all gradients which are consistent with any 2S PSM irradiance pair can be calculated by using equation (39). If we look at the corresponding points on the Gaussian sphere, then every pair of positive irradiances restricts the orientations to a half of a great circle because the latter is represented in the gradient space by a straight line. In contrast to the gradient space the representation of orientations using the Gaussian sphere is independent from the viewer direction $\mathbf{v}$. Therefore, the number of solutions reduces implicitly from a great circle to a half of a great circle since only those orientations are relevant.

The perimeter of the circles can be seen as a measure of the cardinality of the orientations which are consistent with the irradiances. The larger the irradiance value, the smaller the perimeter of the circle. The irradiance E and the perimeter of the circle are related through the equation

$$U = 2\pi \cdot \left(1 - \left(\frac{E}{E_0 \rho}\right)^2\right) . \tag{52}$$

On the other hand, the perimeter of the circle of albedo independent 2S methods remains always equal to 2π for all irradiance pairs and therefore it is in general larger than the circles in SFS methods while keeping the viewer direction and the restriction of the orientations by the illumination directions in mind. Besides the surface orientation another unknown variable, the albedo ρ, exists for 2S methods. Neighboring orientations on the surface are often linked together through smoothness assumptions as discussed in Section 4.1. From a formal point of view such assumptions would also be sensible for the albedo. But for real-world objects discontinuous albedo changes are more likely. Usually discontinuous albedo variations occur more often than smooth color value changes or gray value changes.

Assume that a unique gradient map of a Lambertian surface has to be recovered from a pair of irradiance images without knowing the albedo value ρ. Assume that the two illumination directions $\mathbf{s}_1$ and $\mathbf{s}_2$ are known associated with the irradiance images.

[Lee & Rosenfeld 1985] propose a 3D shape recovery method for Lambertian surfaces that can be approximated locally by spheres. Under the assumption of a locally spherical surface it can be shown that the possible orientations can be restricted to a straight line in the gradient space for a given a single image irradiance value E. This is even possible without knowledge of the $E_0\rho$ term. The restriction to a straight line follows by using the irradiance changes for the considered image point. It can be shown that this straight line can be represented by the equation

$$E_y \cdot p - E_x \cdot q = \tan(\sigma(\mathbf{s})) \cdot (\cos(\theta(\mathbf{s})) \cdot E_y - \sin(\theta(\mathbf{s})) \cdot E_x) \ . \tag{53}$$

As for linear reflectance maps two irradiances are sufficient to recover the gradient $(p, q) = (u_x, u_y)$ uniquely by intersecting two straight lines, for each image point. This solution is not only independent of the albedo ρ, it can be calculated so that the solution becomes independent of the absolute irradiances of the light sources, as well. In practice this makes the determination of the illumination parameters easier. As a conclusion the knowledge of the ratio E_{01}/E_{02} of the irradiances values is sufficient. For the numerical determination of the partial derivatives of the image irradiance function $E(x, y)$ it has to be assumed that the albedo ρ does not change in the immediate neighborhood of an image point.

5 Shape from Shading

The SFS problem is the hardest in the class of shading based shape recovery problems. The given information is a single image E and a reflectance model [Horn 1990, Zhang et. al 1994].

It was shown by [Horn 1986] that the SFS problem for a Lambertian surface with constant albedo corresponds to that of solving the following first-order partial differential equation

$$E(x,y) = \frac{p_1 \cdot u_x + p_2 \cdot u_y - p_3}{\sqrt{p_1^2 + p_2^2 + p_3^2} \cdot \sqrt{u_x^2 + u_y^2 + 1}}, \tag{54}$$

defined over a domain Ω. We consider here the case when the albedo is constant, see (54). Given $0 \leq E(x,y) \leq 1$, the questions of the existence and uniqueness of solutions to (54) arise naturally. Existence corresponds to the problem of whether a given shading pattern with intensity between 0 and 1 is generated by a genuine Lambertian surface. Uniqueness corresponds to that of whether a shading pattern is due to one and only one Lambertian shape (given up to a constant). We shall analyze in this section only the case when $\mathbf{s} = (0,0,-1)$. One can rewrite then (54) as the *eikonal equation*

$$u_x^2 + u_y^2 = \mathcal{E}(x,y) \tag{55}$$

with $\mathcal{E}(x,y) = E(x,y)^{-2} - 1$.

In this section we present first two different classes of images for which there are no genuine shapes. In the second part of this section we refer to the uniqueness problem for the eikonal equation (55). Lastly, we briefly discuss a number of methods recovering the unknown surface from its single image.

5.1 Images without Solution

Let R be either a positive number or $+\infty$. Let f be a non-negative continuous function on the interval $[0,R)$ vanishing exactly at zero. Consider equation (55) with

$$\mathcal{E}(x,y) = f(\sqrt{x^2+y^2}) \tag{56}$$

given over $D(R) = \{(x,y) \in \Re^2 : x^2 + y^2 < R^2\}$. With this special form of image, the class of circularly-symmetric solutions is of the form $\pm U + k$, where

$$U(x,y) = \int_0^{\sqrt{x^2+y^2}} \sqrt{f(\sigma)}\ d\sigma. \tag{57}$$

A condition on f guaranteeing that all solutions to the corresponding eikonal equation are unbounded may readily be formulated. Clearly, in the class of circularly-symmetric solutions, this sufficient condition is

$$\int_0^R \sqrt{f(\sigma)}\, d\sigma = +\infty. \tag{58}$$

It is less evident, though true, that the same condition is sufficient in the general case. In fact, we have the following (see [Brooks et. al 1992]):

Theorem 9 *Let f be a non-negative continuous function on $[0, R)$ vanishing exactly at zero and satisfying (58). Then there is no bounded C^1 solution in $D(R)$ to (55) with E given by $E(x, y) = f(\sqrt{x^2 + y^2})$.*

Interestingly, condition (58) is not only sufficient but also necessary for the unboundedness of all solutions to the equation in question. We have the following theorem (see [Brooks et. al 1992, Brooks et. al 1992a]):

Theorem 10 *Let f be a non-negative continuous function in $[0, R)$ vanishing exactly at zero and satisfying $\int_0^R \sqrt{f(\sigma)}\, d\sigma < +\infty$. Then every solution in $D(R)$ to (55) with $E(x, y) = f(\sqrt{x^2 + y^2})$ is bounded.*

Observe that whether the integral $\int_0^R \sqrt{f(\sigma)}\ d\sigma$ is finite or infinite depends exclusively on the behaviour of f near R. The integral will be infinite if, for example, $f(r)$ diverges to infinity sufficiently rapidly as r tends to R. This means that, in the context of real images of Lambertian surfaces illuminated by an overhead point light-source, a circularly-symmetric image cannot be derived from a genuine shape if it gets dark too quickly as the image boundary is approached.

We now establish the existence of images E for which there is no solution whatsoever to equation (55). See also [Brooks et. al 1992b, Horn et. al 1989].

Theorem 11 *Let Ω be a bounded open connected subset of the $\Re^2$ with boundary $\partial\Omega$ being a piecewise C^1 curve of length $\ell_{\partial\Omega}$. Let (x_0, y_0) be a point in Ω and r be a positive number such that the closed disc $\bar{D}(x_0, y_0, r)$ of radius r centered at (x_0, y_0) is contained in Ω. Suppose E is a non-negative continuous function on the closure of Ω, positive in Ω, such that*

$$4r\sqrt{E_1} > \ell_{\partial\Omega}\sqrt{E_2}, \tag{59}$$

where $E_1 = \min\{E(x, y) : (x, y) \in \bar{D}(x_0, y_0, r)\}$ and $E_2 = \max\{E(x, y) : (x, y) \in \partial\Omega\}$. Then there is no C^1 solution to (55) in Ω.

Note that the theorem is of local character: if Ω is a subset of a domain Δ and E is a non-negative function on Δ whose restriction to Ω satisfies (59) for some choice of $\bar{D}(x_0, y_0, r)$ in Ω, then, obviously, there is no C^1 solution to (55) in Δ. Reformulated in terms of Lambertian shading, this locality property can be expressed as saying that no genuine image can admit too dark a spot on too bright a background, assuming that the background does not contain a point having unit brightness. The precise balance between the qualifications "too dark" and "too bright" is, of course, given by condition (59).

5.2 Ambiguous Shading Patterns

The second part of this section refers to the uniqueness problem for the eikonal equation (55). Uniqueness of this kind has been demonstrated in the case where $E(x,y) = (x^2+y^2)(1-x^2-y^2)^{-1}$. Deift and Sylvester [Deift & Sylvester 1981], proved that $\pm(1-x^2-y^2)^{1/2} + k$ are the only C^2 solutions to this equation over the unit disc $D(1)$. All of these solutions are hemispherical in shape. In an effort to obtain a more general result, [Bruss 1982] asserted the following: if $D(R)$ is the disc in the xy-plane with radius R centered at the origin, and f is a continuous function on $[0,R)$ of class C^2 over $(0,R)$ satisfying the following conditions:

(i) $f(0) = 0$ and $f(r) > 0$ for $0 < r < R$,

(ii) $\lim_{r\to 0} f'(r) = 0$, $\lim_{r\to 0} f''(r)$ exists and is positive,

(iii) $\lim_{r\to R} f(r) = +\infty$,

then all solutions of class C^2 to (55) in $D(R)$ with $E(x,y) = f(\sqrt{x^2+y^2})$ take the form

$$\pm \int_0^{\sqrt{x^2+y^2}} \sqrt{f(\sigma)}\, d\sigma + k, \tag{60}$$

and so are circularly symmetric with common shape. It is possible to show that the above Bruss' Ph.D. claim is invalid (for the construction of the specific counter-example see [Brooks et. al 1992a, Brooks et. al 1992b]). Similarly, in [Kozera 1997a] it was recently shown that Brooks' Ph.D. uniqueness results [Brooks 1983, Brooks 1983a] concerning the images of the Lambertian plane and hemi-sphere have been erroneously proved. Some new uniqueness results have been also established in [Oliensis 1991] and [Rouy & Tourin 1992]. It should be noted, however, that these results introduce additional uniqueness enforcement conditions that cannot be easily obtained as the initial data from a mere single image.

We shall present now a number of surface reconstruction algorithms for a single-image shape recovery and will briefly discuss their intrinsic limitations.

5.3 Method of Characteristic Strips

This method is based on the classical approach from the theory of the first-order partial differential equations applied to the equation

$$F(x,y,u,p,q) = 0, \tag{61}$$

where $F(x,y,u,p,q) = p^2+q^2-\mathcal{E}(x,y)$ over image Ω. This was first introduced in the shape-from-shading literature by [Horn 1986]. For a more detailed theory discussing the general case of F involving n-independent variables, an interested

reader is referred to [John 1971]. We shall briefly now outline the basics of the *method of characteristic strips* in the context of the shape-from-shading problem.

Given an initial curve $\gamma \subset \Re^2$ in the image (image boundary) Ω and surface height over γ, the unknown surface $S(t,s)$ is generated along the so-called *base characteristics* $(x(t,s), y(t,s))$ expressed in a parametric form depending on (t,s)-variables (see the first two equations in (62)). Here, variable s parametrizes initial curve γ and variable t parametrizes the evolution of the surface $S(t,s)$ along base charctersistic direction (*i.e.* whenever s is fixed). Another words, the surface S is swept out by the family of characteristics of the form

$$t \to (x(t,s), y(t,s), u(t,s), p(t,s), q(t,s))$$

satisfying the corresponding system of five ordinary differential equations (called also characteristic equations)

$$\begin{aligned} x_t(t,s) &= 2p(t,s), \\ y_t(t,s) &= 2q(t,s), \\ u_t(t,s) &= 2\mathcal{E}(x(t,s), y(t,s)), \\ p_t(t,s) &= \mathcal{E}_x(x(t,s), y(t,s)), \\ q_t(t,s) &= \mathcal{E}_y(x(t,s), y(t,s)). \end{aligned} \tag{62}$$

It is assumed here that the function u defined over *generalized initial curve* $\widetilde{\gamma} \in R^5$

$$\begin{aligned} x(0,s) &= x_0(s), \\ y(0,s) &= y_0(s), \\ u(0,s) &= u_0(s), \\ p(0,s) &= p_0(s), \\ q(0,s) &= q_0(s) \end{aligned} \tag{63}$$

satisfies an eikonal equation and a chain-rule along $\widetilde{\gamma}$

$$p_0^2(s) + q_0^2(s) = \mathcal{E}(x_0(s), y_0(s)), \tag{64}$$

$$\dot{u}_0(s) = p_0(s)\dot{x}_0(s) + q_0(s)\dot{y}_0(s), \tag{65}$$

and that the curve γ obeys the so-called *non-charcteristic condition*

$$\dot{x}_0 F_q - \dot{y}_0 F_p \neq 0, \tag{66}$$

for all $(x_0(s), y_0(s)) \in \gamma(s)$. The last condition excludes the case when the initial curve γ coincides with the base characteristic direction. In such a situation the solution would collapse to a single curve in $\Re^3$. Note also that, if $p_0(s_0)$ and $q_0(s_0)$ are *a priori* given, then by using implicit function theorem and condition (66) one can find $p_0(s)$ and $q_0(s)$, defined in some neighbourhood of s_0. Assuming that γ is non-characteristic and that F and γ are of class C^2, the following result (due to Cauchy; see *e.g* [John 1971]) can be established:

Theorem 12 *There exists, in some strip neighbourhood of γ, exactly one C^1 solution $(x(t,s),\ y(t,s),\ u(t,s), p(t,s), q(t,s))$ of Cauchy problem* (62) *and* (63) *such that $\widetilde{u}(x(t,s), y(t,s)) = u(t(x,y)\ s(x,y))$ defines a unique C^2 solution to the problem* (61)*.*

With the aid of the above theorem, one can transform a given first-order partial differential equation into an equivalent system of five mutually coupled ordinary differential equations. Such transformation, in general, renders still a diffucult task for finding an exact analytic solution to a corresponding Cauchy problem (62) and (63). To see it, note that the unknown functions appearing in left-hand sides of (62), reappear also in the right-hands of the same system in a non-linear form. The alternative, is to resort *e.g.* to the finite-difference approximations of the derivatives applied to the left-hand sides of the system (62). Consequently, by using a forward-difference derivative approximation, the following sequential scheme can be derived:

$$\begin{aligned} x(t^{n+1}, s^k) &= x(t^n, s^k) + 2\Delta t p(t^n, s^k), \\ y(t^{n+1}, s^k) &= y(t^n, s^k) + 2\Delta t q(t^n, s^k), \\ u(t^{n+1}, s^k) &= u(t^n, s^k) + 2\Delta t \mathcal{E}(x(t^n, s^k), y(t^n, s^k)), \\ p(t^{n+1}, s^k) &= p(t^n, s^k) + \Delta t \mathcal{E}_x(x(t^n, s^k), y(t^n, s^k)), \\ q(t^{n+1}, s^k) &= q(t^n, s^k) + \Delta t \mathcal{E}_y(x(t^n, s^k), y(t^n, s^k)), \end{aligned} \tag{67}$$

where each (t^n, s^k) represents the corresponding point on the grid expressed in (t,s) coordinate system. It is clear that given the scheme (67) and Dirichlet and Neumann boundary conditions (63) one can sequentially find a numerical solution to (62). The following convergence and stability results for the above numerical scheme can be established (see *e.g* [Gear 1971]):

Theorem 13 *Assume that function $\mathcal{E} \in C^2(\bar{\Omega})$ is defined over compact $\bar{\Omega}$. Then, if $0 \leq t \leq b$, the numerical solution to* (67) *is convergent to the solution $(x(t,s), y(t,s),\ u(t,s), p(t,s),\ q(t,s))$ of the Cauchy problem* (62) *and* (63)*. Moreover, a corresponding finite-difference scheme* (67) *is stable with the stability upper-bound constant equal to e^{bL}, where*

$$\alpha_1 = 2 \sup_{(x,y)\in\Omega} \{|\mathcal{E}_x(x,y)| + |\mathcal{E}_y(x,y)|\}, \quad \alpha_2 = \sup_{(x,y)\in\Omega} \{|\mathcal{E}_{xx}(x,y)| + |\mathcal{E}_{yx}(x,y)|\},$$

$$\alpha_3 = \sup_{(x,y)\in\Omega} \{|\mathcal{E}_{xy}(x,y)| + |\mathcal{E}_{yy}(x,y)|\},$$

and constant $L = \max_{1\leq i\leq 3}\{2, |\alpha_i|\}$. Finally, the scheme (67) *is absolutely stable, if $|1 + \Delta t L| \leq 1$.*

The main problem with the method of characteristic strips stems out from the fact that the surface should not be reconstructed over (t,s) coordinate system but in the standard cartesian (x,y) coordinate system. The corresponding transformation between two coordinate systems usually changes the rectangular

grid (expressed in (t,s) variables) to the curvilinear cartesian grid. Hence, the coverage of the image domain by base characterstics $(x(t,s),y(t,s))$ tends to be uneven, resulting in a inhomogeneous density of the reconstructed surface. The next problem is that the coverage of the image domain will only be extensive if the initial curve and surface are appropriately chosen. Furthermore, the method is not amenable to parallelism and should not be applied in the neighbourhood of the occluding boundary, where constant $L = \infty$. Note, however, that for any fixed constant L, a strong stability condition can be enforced by shrinking Δt, respectively. The latter assures that the computed numerical solution to (67) is "close" to the ideal solution to (67), and thus, by the last convergence result, "close" to the solution of the Cauchy problem (62) and (63). Finally, it should be pointed out that method of characteristic strips requires Dirichlet and Neumann boundary conditions which, in case if not *a priori* given, might not be easily obtainable from a mere image Ω.

We close this section with an example illustrating some difficulties which might appear in solving analyticly the Cauchy problem (62) and (63), even in special simple cases of eikonal equation.

Example 5 Consider the following eikonal equation

$$u_x^2(x,y) + u_y^2(x,y) = c, \tag{68}$$

where $c > 0$ is an arbitrary constant. With no extra bounadry conditions the problem is ill-posed as the family of functions $v(x,y) = ax+by$, where $a^2+b^2 = c$, constitutes different C^2 class solutions to (68). Let us now incorporate Dirichlet and Neumann boundary conditions along the $Y-$axis: $v(0,y) = \bar{b}y$, $v_x(0,y) = \bar{a}$, and $v_y(0,y) = \bar{b}$, where $(\bar{a},\bar{b}) \neq (0,0)$, $\bar{a} \neq 0$, and $\bar{a}^2+\bar{b}^2 = c$. The corresponding Cauchy problem (62) and (63) takes the following form:

$$\begin{aligned}
(a)\ x_t(t,s) &= 2p(t,s), \\
(b)\ y_t(t,s) &= 2q(t,s), \\
(c)\ u_t(t,s) &= 2c, \\
(d)\ p_t(t,s) &= 0, \\
(e)\ q_t(t,s) &= 0,
\end{aligned} \tag{69}$$

with the corresponding boundary conditions defined as

$$\begin{aligned}
(a)\ x(0,s) &= 0, \\
(b)\ y(0,s) &= s, \\
(c)\ u(0,s) &= \bar{b}s, \\
(d)\ p(0,s) &= \bar{a}, \\
(e)\ q(0,s) &= \bar{b}.
\end{aligned} \tag{70}$$

Note that the conditions (64), (65), and (65) are here clearly satisfied. Furthermore, $(69)(d,e)$ combined with $(70)(d,e)$ yields $p(t,s) = \bar{a}$ and $q(t,s) = \bar{b}$. By

coupling (69)(a) and (70)(a) together with (69)(b) and (70)(b) we obtain that $x(t,s) = 2\bar{a}t$ and $y(t,s) = 2\bar{b}t + s$. Thus, $t(x,y) = x/2\bar{a}$ and $s(x,y) = y - (\bar{b}/\bar{a})x$. With the aid of (69)$(c)$ and (70)(c) we arrive at $u(t,s) = ct + \bar{b}s$. Putting $t(x,y)$ and $s(x,y)$ back into $u(t,s)$, and bearing in mind that $c = \bar{a}^2 + \bar{b}^2$, we finally obtain $u(t,s) = \widetilde{u}(x(t,s), y(t,s)) = \bar{a}x + \bar{b}y$. Theorem 12 assures also, that the latter forms a unique C^2 class solution to Cauchy problem (69) and (70). A moment reflection reveals, however, that finding an exact analytic solution for $u_x^2(x,y) + u_y^2(x,y) = x^2 + y^2$, by using the method of characteristic strips, is much more complicated.

5.4 Method of Equal-height Contours

This method is a variant of the method of characteristic strips. Namely, it is assumed here that $\gamma(s)$, (where $s \in (a,b)$) is a smooth (piecewise smooth) *equal-height contour* contained in the image Ω (*i.e.* $\widetilde{u}(x,y) = C$ over γ). By imposing such special Dirichlet boundary conditions it is possible to determine the Neumann boundary conditions, up to two pairs of gradient defined along curve γ. In case of equal-height contour a corresponding solution $\widetilde{u}$ is generated along the evolution of equal-height contours γ_t, for which $\gamma_0 = \gamma$. Another words, the unknown surface is swept out by $(\gamma_t, \widetilde{u}(\gamma_t))$, where the family $\gamma_t(s) = \{(x(t,s), y(t,s)) : (s,t) \in (a,b) \times (c,d)\}$ of equal-height contours is generated by solving the following Cauchy problem:

$$\begin{aligned} x_t(t,s) &= \pm \frac{y_s(t,s)}{\sqrt{\mathcal{E}(x(t,s), y(t,s))(x_s^2(t,s) + y_s^2(t,s))}}, \\ y_t(t,s) &= \mp \frac{x_s(t,s)}{\sqrt{\mathcal{E}(x(t,s), y(t,s))(x_s^2(t,s) + y_s^2(t,s))}}, \\ x(0,s) &= x_0(s), \\ y(0,s) &= y_0(s), \end{aligned} \tag{71}$$

and $\gamma_0(s) = (x(0,s), y(0,s))$ is the initial equal-height contour. A final solution $\widetilde{u}$ is given here by

$$\widetilde{u}(x(t,s), y(t,s)) = u(t,s) = t + C, \tag{72}$$

where $u(0,s) = C$. The choice of appropriate pair of signs $(+,-)$ or $(-,+)$ in formulae (71), governs the direction of evolution of equal-height contours (either outwards or inwards).

Note that, if we differentiate $\widetilde{u}(x(t,s), y(t,s)) = t$ over the parameter s, the chain rule yields $p(t,s)x_s(t,s) + q(t,s)y_s(t,s) = 0$. This combined with the fact that $p^2(t,s) + q^2(t,s) = \mathcal{E}(x(t,s), y(t,s))$ implies that

$$p(t,s) = \pm \frac{y_s(t,s)\sqrt{\mathcal{E}(x(t,s), y(t,s))}}{\sqrt{x_s^2(t,s) + y_s^2(t,s)}} \quad \text{and}$$

$$q(t,s) = \mp \frac{x_s(t,s)\sqrt{\mathcal{E}(x(t,s),y(t,s))}}{\sqrt{x_s^2(t,s)+y_s^2(t,s)}}. \tag{73}$$

In particular, for $s=0$, there exist exactly two choices of Neumann boundary conditions guaranteeing, in each case, the existence of a unique C^2 class solution to a corresponding Cauchy problem (see Theorem 12). Indeed, let u be a C^2 class solution to problem (71) and (72) with Dirichlet boundary condition set to $u(\gamma) = C$. An easy inspection shows that function $v = -u + 2C$ satisfies $u_x^2 + u_y^2 = \mathcal{E}(x,y)$, Dirichlet boundary conditions $v(\gamma) = C$, and one of the Neumann boundary conditions (73). Thus, we have *an essential duality* in solving a Cauchy problem (71) and (72), which is ambiguous up to a vertical shift and mirror-like reflection.

Note, that (71), (72), and (73) can be transformed into an equivalent system of five characteristic strip equations:

$$\begin{aligned}
x_t(t,s) &= \frac{p(t,s)}{p^2(t,s)+q^2(t,s)},\\
y_t(t,s) &= \frac{q(t,s)}{p^2(t,s)+q^2(t,s)},\\
u_t(t,s) &= 1,\\
p_t(t,s) &= \frac{\mathcal{E}_x(x(t,s),y(t,s))}{2(p^2(t,s)+q^2(t,s))},\\
q_t(t,s) &= \frac{\mathcal{E}_y(x(t,s),y(t,s))}{2(p^2(t,s)+q^2(t,s))}.
\end{aligned} \tag{74}$$

The last system differs from the system of characteristic strips by the speed of evolution along the base charctersitic direction. Thus, both systems are equivalent and render the same solution. This variant of the method of characteristic strips was mentioned in shape-from-shading literature by [Bruckstein 1988] and later re-introduced by [Kimmel & Bruckstein 1994]. For a more detailed mathematical analysis of this method an interested reader is also referred here to [Osher 1993, Sethian 1985]. The corresponding discrete method of equal-height contour evolution is analyzed by [Osher & Sethian 1988, Sethian 1990]. Recently, *a Fast Marching Level Set Method* has been applied to the eikonal equation over a rectangular grid [Sethian 1996]. An interested reader is also referred to [Kozera & Klette 1997], where convergence, stability, and performance of various finite-difference schemes (applied over a rectangular grid to the linear shape from shading problem) have been discussed.

Note finally, that the knowledge of the initial equal-height contour (which is a clear drawback of this method), as opposed to the general case of extracting general Dirichlet and Neumann boundary conditions (necessary for applying a method of characteristic strips) can, in certain cases, be obtainable. The latter happens *e.g.*, if the surface is positioned on the horizontal plane and disappears continuously from the viewing direction.

We shall close this subsection with an example illustrating the equal-height contour method.

Example 6 Consider the eikonal equation introduced in (68). Let the initial height-contour $\gamma_0(s)$ be $x(0,s) = s/a$, $y(0,s) = -s/b$, along which $u(0,s) = 0$, and $ab \neq 0$. We search for $\widetilde{u}(x(t,s), y(t,s)) = u(t,s) = t$, where the pair $(x(t,s), y(t,s))$ satisfies the following system:

$$\begin{aligned} x_t(t,s) &= \frac{-y_s(t,s)}{\sqrt{c(x_s^2(t,s) + y_s^2(t,s))}}, \\ y_t(t,s) &= \frac{x_s(t,s)}{\sqrt{c(x_s^2(t,s) + y_s^2(t,s))}}. \\ u(t,s) &= t \\ x(0,s) &= x_0(s), \\ y(0,s) &= y_0(s). \end{aligned} \tag{75}$$

In order to solve (75), pertinent Neumann boundary conditions have to be incorporated. Choosing in (73) a pair $(-,+)$ we obtain:

$$p(t,s) = \frac{-y_s(t,s)\sqrt{c}}{\sqrt{x_s^2(t,s) + y_s^2(t,s)}} \quad \text{and} \quad q(t,s) = \frac{x_s(t,s)\sqrt{c}}{\sqrt{x_s^2(t,s) + y_s^2(t,s)}}.$$

Thus $p(0,s) = a$ and $q(0,s) = b$ along initial equal-height contour $\gamma_0(s)$ and therefore the last two equations of (74) yields $p(t,s) = a$ and $q(t,s) = b$. This, together with the first two equations of (74) yields $x(t,s) = (a/c)t + s/a$ and $y(t,s) = (b/c)t - s/b$. Hence, $t(x,y) = ax + by$. As $\widetilde{u}(x(t,s), y(t,s)) = u(t,s) = t$ we finally arrive at one of two C^2 class solution to (75). Choosing, in turn, the second pair $(+,-)$ in (73) we obtain the second C^2 class solution $\widetilde{v}(\bar{x}(t,s), \bar{y}(t,s)) = -a\bar{x} - b\bar{y}$ to problem (75).

5.5 Direct Variational Method

The methods of [Horn 1986] and [Bruckstein 1988] rely in a crucial way on provision of prior information (Dirichlet or Neumann boundary conditions). The amount of necessary information usually exceeds the minimal amount of initial data required by various theoretical uniqueness results. This is so because the algorithms based on differential equations cannot proceed by starting from singular points (*i.e.* for the point for which $\mathcal{E}(x_0, y_0) = 0$) which, as it turns out, are important clues for the shape recovery process.

In this section we shall only outline *a direct variational method* by analysing the simpliest case. For a more general case see [Brooks & Chojnacki 1994]. We assume here that a domain Ω has exactly *one singular point* $S_0 = (x_0, y_0)$. A direct variational method discussed in [Brooks & Chojnacki 1994] is based on the following crucial result.

Theorem 14 *If a function u satisfies an eikonal equation* (55) *over a domain Ω, and X and Y are points in Ω that can be joined by the base characteristic curve wholly contained in Ω, then the relative depth $|u(X) - u(Y)|$ bewteen points*

of the graph of u is given by

$$|u(X) - u(Y)| = \min_{\gamma} \int_{\gamma} \sqrt{\mathcal{E}} dl, \tag{76}$$

where the minimum is taken over all piecewise smooth curves γ in Ω joining X and Y, and the integration is meant with respect to standard measure.

The proof of Theorem 14 reveals that a minimal value of (76) is attained along the base characteristic direction (*i.e.* along gradient direction). It can be shown that for the *convex (concave)* Lambertian surface the corresponding image has exactly one singular point S_0 (where $u_x(S_0) = u_y(S_0) = 0$) and that each point of the image $X \in \Omega$ can be joined by the base characteristic curve with S_0. Consequently, the previous theorem yields:

$$u(X) = u(S_0) - \min_{\gamma} \int_{\gamma} \sqrt{\mathcal{E}} dl \quad \text{and} \quad u(X) = u(S_0) + \min_{\gamma} \int_{\gamma} \sqrt{\mathcal{E}} dl, \tag{77}$$

whenever the surface is convex/concave. Note that, for the saddle-like function $u(x, y) = xy$ the base characteristic pattern (which in case of arbitrary eikonal equation coincides with the gradient direction) does not have the above property. Consequently, the method presented here can only be applicable to the convex (concave) surfaces. In an effort of extending this result for an image containing more than one singular point a generalization of the notion of the convex (concave) surface is necessary. It is useful at this stage to consider those smooth surfaces having base characteristic curves pointing outward (or inward) at the periphery of the domain. They are called *convex skirt* surfaces (see [Brooks & Chojnacki 1994] or [Oliensis 1991]). In addition, it is assumed that the convex skirt function, in the neighbourhood of the singular point S_0, has a non-vanishing Hessian. By using *index theory* (see [Brooks & Chojnacki 1994]) it can be shown that the number of singular points has to be odd. Moreover, if N_+ denotes the number of concave singular surface points, N_- denotes the number of convex singular surface points, and $N_\pm$ denotes the number of saddle singular surface points then it can be shown that any convex skirt surface with non-vanishing Hessian has to satisfy the following condition $N_+ + N_- - N_\pm = 1$. The latter imposes a clear constraint on the number of possible solutions. For $n = 1$, we have only two possible cases: $N_+ = 1$ together with its morror-like reflection $N_- = 1$. For the case when $n = 3$, there are four possible solutions. An interested reader is referred here to [Brooks & Chojnacki 1994], where a method of finding a convex skirt solution (generalizing Theorem 14) together with explicit shape recovery algorithm is presented. A similar topic is also discussed by [Oliensis & Dupuis 1993].

Finally, we point out that in order to derive a computational scheme for (77) Dijkstra's greedy algorithm for finding the shortest path from the single source to any other node on a weighted graph can be used [Cormen et. al 1990]. The source here, will be a singular point S_0, the nodes of the graph coincide with the rectangular grid points and the edges are the straight lines joining the

eight neihgbouring points with any point at the grid. Assuming that the grid increment is h, the corresponding weigth function ω assigned to each existing edge $((x_i, y_j), (x_k, y_l))$ can be defined as:

$$\omega((x_i, y_j), (x_k, y_l)) = \begin{cases} \frac{h}{2}(\sqrt{\mathcal{E}(x_i, y_j)} + \sqrt{\mathcal{E}(x_k, y_l)}), & \text{if } |k-i| + |l-j| = 1, \\ \frac{h}{\sqrt{2}}(\sqrt{\mathcal{E}(x_i, y_j)} + \sqrt{\mathcal{E}(x_k, y_l)}), & \text{if } |k-i| + |l-j| = 2. \end{cases} \tag{78}$$

For more detailed analysis concerning numerical schemes for (77) an interested reader is refered to [Brooks & Chojnacki 1994] and [Cormen et. al 1990].

The use of the above optimization method reduces the number of initial information necessary to ascertain well-posedness of a given shape-from-shading problem (*e.g* no boundary conditions are here requested). Similarly to the case of photometric stereo, the unknown function u is found, up to an arbitray constant. In addition, the computational scheme for (77) can be derived over a fixed rectangular grid. The major disadvantage stems out, however, from the necessity of tightening the originial class of C^1 class surfaces to convex/concave skirt C^1 class surfaces. Such a restriction appears neither in photometric stereo nor in other single image shape reconstruction algorithms. The latter is, however, achieved by imposing additional constraints such as multiple illuminations or accessibility of boundary conditions.

6 Concluding Remarks

SFS methods require a strong restriction of the object surfaces because the problem to recover a surface from a single image is extremely underdetermined. Therefore, SFS is an ill-posed problem. Assumptions on the surface properties support to find a unique solution to a certain extent. But with every additional restriction the practical use of such methods declines as well. Very critical simplifications are the following three assumptions.

(i) The term $E_0\rho$ is known and constant.

(ii) The surfaces are at least C^1-continuous.

(iii) 3D coordinates of singular points and/or singular orientations are known.

This TR informed about 2S and 3S PSM techniques which allow to refrain from assumptions (i) and (iii). Assumption (ii) is also related to the discrete integration problem as briefly discussed in Section 2.3. PSM techniques can be improved further by using colored light sources [Woodham 1994, Drew 1994], or by integration of shadow information [Solomon & Ikeuchi 1996, Schlüns 1997]. This TR also informed about theoretical work, and here we can state a situation where SFS or albedo dependent 2S PSM are analysed at greater detail as 3S PSM so far. However there exist more contributions to fundamentals of 3S PSM as cited in this TR.

In comparison to different shape recovery techniques (for a detailed description of different techniques see, e.g., [Klette et. al 1998]), as based on structured lighting, or on motion and occluding boundaries, shading based shape recovery has special benefits (use of inexpensive equipment, no dangerous radiation). It offers reasonable accuracy and time-efficient reconstructions for selected applications.

References

[Brooks 1983] M. J. Brooks. Shape from shading discretely. *Ph.D. Thesis*, Essex University, England, 1983.

[Brooks 1983a] M. J. Brooks. Two results concerning ambiguity in shape from shading. In: *Proc. Nat. Conf. on Artificial Intelligence*, pp. 26-39, Washington D.C., U.S.A., 1983.

[Brooks et. al 1992] M. J. Brooks, W. Chojnacki, and R. Kozera. Shading without shape. *Quarterly of Applied Mathematics*, 50(1):27-38, 1992.

[Brooks et. al 1992a] M. J. Brooks, W. Chojnacki, and R. Kozera. Circularly symmetric eikonal equations and non-uniqueness in computer vision. *J. Math. Analysis and Applications*, 165(1):192-215, 1992.

[Brooks et. al 1992b] M. J. Brooks, W. Chojnacki, and R. Kozera. Impossible and ambiguous shading patterns. *Internat. J. Computer Vision*, 7(2):119-126, 1992.

[Brooks & Chojnacki 1994] M. J. Brooks and W. Chojnacki. Direct computation of shape from shading. In: *Proceedings 12th Internat. Conf. Pattern Recognition*, pp. 114-119, Jerusalem, Israel, 1994.

[Bruckstein 1988] A. M. Bruckstein. On shape from shading. *Computer Vision, Graphics and Image Processing*, 44(2):139-154, 1988.

[Bruss 1982] A. R. Bruss. The eikonal equation: some results applicable to computer vision. *J. Math. Physics*, 23(5):890-896, 1982.

[Cormen et. al 1990] T. H. Cormen, C. E. Leiserson, and R. L. Rivest. *Introduction to algorithms*. Cambridge, MA, MIT Press, 1990.

[Deift & Sylvester 1981] P. Deift and J. Sylvester. Some remarks on the shape-from-shading problem in computer vision. *J. Math. Analysis and Applications*, 84(1):235-248, 1981.

[Drew 1994] M. S. Drew. Robust specularity detection from a single multi-illuminant color image. *CVGIP: Image Understanding*, 59:320-327, 1994.

[Foley et. al 1990] J. D. Foley, A. van Dam, S. K. Feiner, and J. F. Hughes. *Computer Graphics - Principles and Practice*. 2nd ed., Addison-Wesley, Reading, Massachusetts, 1990.

[Frankot & Chellappa 1988] R. T. Frankot and R. Chellappa. A method for enforcing integrability in shape from shading algorithms. *IEEE Trans. on Patt. Anal. and Mach. Int.*, PAMI-10:439-451, 1988.

[Gear 1971] C. W. Gear. *Numerical initial value problems in ordinary differential equations*, Englewood Cliffs, New Jersey, Prentice-Hall Inc., 1971.

[Haralick & Shapiro 1993] R. M. Haralick and L. G. Shapiro. *Computer and Robot Vision*. Vol. II, Addison-Wesley, Reading, Massachusetts, 1993.

[Hashimoto et. al 1995] Y. Hashimoto, M. Yamamoto and T. Asaida. Cameras and display systems. *Proc. IEEE*, 83:1032-1043, 1995.

[Hecht 1997] E. Hecht. *Optics*. 3rd ed, Addison-Wesley, Reading, Massachusetts, 1997.

[Horn 1977] B. K. P. Horn. Understanding image intensities. *Artificial Intelligence*, 8:201-231, 1977.

[Horn & Sjoberg 1979] B. K. P. Horn and R. W. Sjoberg. Calculating the reflectance map. *Applied Optics*, 18:1770-1779, 1979.

[Horn 1986] B. K. P. Horn. *Robot vision*, Cambridge, MA, MIT Press, 1986.

[Horn & Brooks 1989] B. K. P. Horn and M. J. Brooks. *Shape from Shading*. The MIT Press, Cambridge, Massachusetts, 1989.

[Horn et. al 1989] B. K. P. Horn, R. Szeliski, and A. Yuille. *Private communication*, 1989.

[Horn 1990] B. K. P. Horn. Height and gradient from shading. *Int. J. of Computer Vision* 5:37-75, 1990.

[John 1971] F. John. *Partial differential equation*, Volume 1, New York, Springer Verlag, 1971.

[Kimmel & Bruckstein 1994] R. Kimmel and A.M. Bruckstein. Tracking level set by level sets: a method for solving the shape from shading problem. *Computer Vision and Image Understanding*, 62(2):47-58, 1994.

[Kimmel & Bruckstein 1995] R. Kimmel and A.M. Bruckstein. Global shape from shading. *Computer Vision and Image Understanding*, 62(3):360-369, 1995.

[Kimmel et al. 1995] R. Kimmel, K. Siddiqi, B. B. Kimia, and A. M. Bruckstein. Shape from shading: level set propagation and viscosity solution. *Int. J. of Computer Vision*, 16:107-133, 1995.

[Klette & Schlüns 1996] R. Klette, K. Schlüns. Height data from gradient fields. In: *SPIE Proc. Photonics East Vol. 2908*, pp. 204-215, Boston, U.S.A., 1996.

[Klette et. al 1998] R. Klette, K. Schlüns, and A. Koschan. *Computer Vision - Spatial Data from Images*. Springer, Singapore 1998 (German edition: Vieweg, Wiesbaden 1996).

[Klinker et. al 1988] G. J. Klinker, S. A. Shafer, and T. Kanade. The measurement of highlights in color images. *Int. J. Computer Vision*, 2:7-32, 1988.

[Klinker et. al 1990] G. J. Klinker, S. A. Shafer, and T. Kanade. A physical approach to color image understanding. *Int. J. Computer Vision*, 4:7-38, 1990.

[Kozera 1991] R. Kozera. Existence and uniqueness in photometric stereo. *Applied Mathematics and Computation*, 44(1):1-103, 1991.

[Kozera 1992] R. Kozera. On shape recovery from two shading patterns. *Internat. J. Pattern Recognition and Artificial Intelligence*, 6(4):673-698, 1992.

[Kozera & Klette 1997] R. Kozera and R. Klette. Finite difference based algorithms for a linear shape from shading. *Machine Graphics and Vision*, 6(2):157-201, 1997.

[Kozera 1997] R. Kozera. A note on complete integrals and uniqueness in shape from shading. *Applied Mathematics and Computation*, 73(1):1-37, 1995.

[Kozera 1997a] R. Kozera. Uniqueness in shape from shading revisited. *J. Math. Imaging and Vision*, 7(2):123-138, 1997.

[Lee & Rosenfeld 1984] C. - H. Lee and A. Rosenfeld. An approximation technique for photometric stereo. *Pattern Recognition Letters*, 2:339-343, 1984.

[Lee & Rosenfeld 1985] C. - H. Lee and A. Rosenfeld. Improved methods of estimating shape from shading using the light source coordinate system. *Artificial Intelligence*, 26:125-143, 1985.

[Lenz 1989] R. Lenz. Image data acquisition with CCD cameras. In: A. Gruen and H. Kahmen (eds.). *Optical 3-D Measurement Techniques*, pp.22-34, Wichmann, Karlsruhe, Germany, 1989.

[McCamy et. al 1976] C. S. McCamy, H. Marcus, and J. G. Davidson. A color-rendition chart. *J. Applied Photographic Engineering.* 2:95-99, 1976.

[Meyer 1988] G. W. Meyer. Wavelength selection for synthetic image generation. *Computer Vision, Graphics and Image Processing.* 41:57-79, 1988.

[Nayar et. al 1991] S. K. Nayar, K. Ikeuchi, and T. Kanade. Shape from interreflections. *Int. J. Computer Vision*, 6:173-195, 1991.

[Nayar & Oren 1995] S. K. Nayar and M. Oren. Generalization of the Lambertian Model and Implications for Machine Vision. *Int. J. Computer Vision*, 14:227-251, 1995.

[Nicodemus et. al 1977] F. E. Nicodemus, J. C. Richmond, J. J. Hsia, I. W. Ginsberg, and T. Limperis. *Geometrical Considerations and Nomenclature for Reflectance.* Monograph 160, U.S. Department of Commerce, National Bureau of Standards, Washington, 1977.

[Oliensis 1991] J. Oliensis. Uniqueness in shape from shading. *International Journal of Computer Vision*, 6(2):75-104, 1991.

[Oliensis & Dupuis 1993] J. Oliensis and P. Dupuis. A global algorithm for shape from shading. In: *Proceedings Internat. Conf. on Comuter Vision*, pp. 692-701, Berlin, Germany, 1993.

[Onn & Bruckstein 1990] R. Onn and A. M. Bruckstein. Integrability disambiguates surface recovery in two-image photometric stereo. *Internat. J. Computer Vision*, 5(1):105-113, 1990.

[Osher & Sethian 1988] S. J. Osher and J. A. Sethian. Fronts propagating with curvature dependent speed: algorithms based on Hamilton-Jacobi formulations. *J. Computational Physics*, 79:12-49, 1988.

[Osher 1993] S. J. Osher. A level set formulation for the solution of the Dirichlet problem for Hamilton-Jacobi equations. *SIAM J. Math. Analysis*, 24(5):1145-1152, 1993.

[Rouy & Tourin 1992] E. Rouy and A. Tourin. A viscosity solutions approach to shape-from-shading. *SIAM Journal on Numerical Analysis*, 29:867-884, 1992.

[Rumpel & Schlüns 1995] D. Rumpel and K. Schlüns. Szenenanalyse unter Berück–sichtigung von Interreflexionen und Schatten. In: *Proc. DAGM-Symposium*, pp. 218-227, Bielefeld, Germany, 1995.

[Schlick 1994] C. Schlick. A survey of shading and reflectance models. *Computer Graphics Forum*, 13:121-131, 1994.

[Schlüns & Teschner 1995] K. Schlüns and M. Teschner. Fast separation of reflection components and its application in 3D shape recovery. In: *Proc. IS&T/SID 3rd Color Imaging Conf.*, pp. 48-51, Scottsdale, Arizona, U.S.A., 1995.

[Schlüns 1997] K. Schlüns. Shading Based 3D Shape Recovery in the Presence of Shadows. In: *Proc. Intern. Conf. on Digital Image & Vision Computing*, pp. 195-200, Albany, Auckland, New Zealand, 1997.

[Sethian 1985] J. A. Sethian. Curvature and the evolution of fronts. *Communications in Mathematical Physics*, 101:487-499, 1985.

[Sethian 1990] J. A. Sethian. Numerical algorithms for propagating interfaces: Hamilton-Jacobi equations and conservation laws. *Journal of Differential Geometry*, 31:131-161, 1990.

[Sethian 1996] J. A. Sethian, *Level set methods: evolving interfaces in geometry, fluid mechanics, computer vision and material science,* Cambridge, Cambridge University Press, 1996.

[Solomon & Ikeuchi 1996] F. Solomon and K. Ikeuchi. Extracting the Shape and Roughness of Specular Lobe Objects Using Four Light Photometric Stereo. *IEEE Trans. Pattern Analysis and Machine Intelligence*, 18:449-454, 1996.

[Woodham 1978] R. J. Woodham. Photometric stereo: a reflectance map technique for determining surface orientation from image intensity. *Image Understanding Systems & Industrial Applications, SPIE*, 155:136-143, 1978.

[Woodham 1994] R. J. Woodham. Gradient and curvature from the photo–metric-stereo method, including local confidence estimation. *J. Optical Society America*, A 11:3050-3068, 1994.

[Zhang et. al 1994] R. Zhang, P. - S. Tsai, J. E. Cryer, and M. Shah. Analysis of shape from shading techniques. In: *Proc. Computer Vision and Pattern Recognition*, pp. 377-384, Seattle, Washington, U.S.A., 1994.